Making the Case for High Temperature Low Sag (HTLS) Overhead Transmission Line Conductors

by

Koustubh Banerjee

A Thesis Presented in Partial Fulfillment
of the Requirements for the Degree
Master of Science

Approved January 2014 by the
Graduate Supervisory Committee:

Ravi Gorur, Chair
George Karady
Raja Ayyanar

ARIZONA STATE UNIVERSITY

May 2014

ABSTRACT

The future grid will face challenges to meet an increased power demand by the consumers. Various solutions were studied to address this issue. One alternative to realize increased power flow in the grid is to use High Temperature Low Sag (HTLS) since it fulfills essential criteria of less sag and good material performance with temperature. HTLS conductors like Aluminum Conductor Composite Reinforced (ACCR) and Aluminum Conductor Composite Core (ACCC) are expected to face high operating temperatures of 150-200 degree Celsius in order to achieve the desired increased power flow. Therefore, it is imperative to characterize the material performance of these conductors with temperature. The work presented in this thesis addresses the characterization of carbon composite core based and metal matrix core based HTLS conductors.

The thesis focuses on the study of variation of tensile strength of the carbon composite core with temperature and the level of temperature rise of the HTLS conductors due to fault currents cleared by backup protection. In this thesis, Dynamic Mechanical Analysis (DMA) was used to quantify the loss in storage modulus of carbon composite cores with temperature. It has been previously shown in literature that storage modulus is correlated to the tensile strength of the composite. Current temperature relationships of HTLS conductors were determined using the IEEE 738-2006 standard. Temperature rise of these conductors due to fault currents were also simulated. All simulations were performed using Microsoft Visual C++ suite. Tensile testing of metal matrix core was also performed.

Results of DMA on carbon composite cores show that the storage modulus, hence tensile strength, decreases rapidly in the temperature range of intended use. DMA on composite cores subjected to heat treatment were conducted to investigate any changes in the variation of storage modulus curves. The experiments also indicates that carbon composites cores subjected to temperatures at or above 250 degree Celsius can cause permanent loss of mechanical properties including tensile strength. The fault current temperature analysis of carbon composite based conductors reveal that fault currents eventually cleared by backup protection in the event of primary protection failure can cause damage to fiber matrix interface.

DEDICATION

To my parents for their love and support.

ACKNOWLEDGMENTS

This thesis would not have been possible without the help and guidance of my advisor, Dr. Ravi Gorur. His knowledge and advice were instrumental in my successfully completing this work. I would like to acknowledge Power System Engineering Research Center (PSERC) for providing me an opportunity to work on HTLS conductor technology.

I am grateful to Professor Shahirar Anwar for providing me access to the material science laboratory, where I performed my thermal mechanical analysis experiments. I appreciate the time he took to train me on the TMA instrument. I would like to thank Professor Lenore Dai, who advised me on dynamic mechanical analysis experiments. It was particulary kind of her to allow me to use the DMA instrument for my work. I would also like to thank her graduate students Haobo Chen and Prithwish Chatterjee for training me on the DMA instrument and providing me indispensable assistance.

I am most grateful to Dr. Dallas Kingsbury for providing critical support and help in tensile testing of HTLS conductors. The custom grips for tensile tests would not have been possible without his help and insight.

I would also like to thank the ASU machine shop for helping me with the samples required for my experiments. I gratefully acknowledge the use of facilities within the Center for Solid State Science at Arizona State University.

My fellow graduate students and colleagues in electric power and energy systems, especially Xianda Deng and Manish Kumar, have been very helpful and supportive of my work. Last but not the least; I would like to thank all my friends for their encouragement and support.

TABLE OF CONTENTS

Page

LIST OF TABLES

Table Page

LIST OF FIGURES

NOMENCLATURE

$A^{'}$	Projected area of the conductor per unit length
AAAC	All Aluminum Alloy Conductor
AAC	All Aluminum Conductor
ACCC	Aluminum Conductor Composite Core
ACCR	Aluminum Conductor Composite Reinforced
ACSR	Aluminum Conductor Steel Reinforced
ACSS	Aluminum Conductor Steel Supported
CFRP	Carbon Fiber Reinforced Plastic
CIGRE	International Council on Large Electric Systems (English)
CTC	Composites Technologies Corporation
CTE	Coefficient of thermal expansion
D	Conductor diameter
DMA	Dynamic Mechanical Analysis
DSC	Differential Scanning Calorimetry
E	Complex modulus of visco-elastic material
$E^{'}$	Storage modulus of visco-elastic material
$E^{''}$	Loss modulus of visco-elastic material
$E_T^{'}$	Storage modulus of carbon fiber/epoxy composite at temperature T
$E_{To}^{'}$	Storage modulus of carbon fiber/epoxy composite at temperature T_o
EHV	Extra High Voltage
G	Shear modulus of visco-elastic material

G	Shear modulus of CFRP at temperature T and time to relaxation t_r
G_g	Shear modulus of CFRP in the glassy region
GBIP	General Purpose Instrument Bus
GLS	Global Load Sharing
GTACSR	Gap Type Aluminum Conductor Steel Reinforced
H_c	Altitude of the sun
HTLS	High Temperature Low Sag
I	Conductor current
IEEE	Institute of Electrical and Electronic Engineers
k	Point of measurement
K_{angle}	Wind direction factor
K_f	Thermal conductivity of air at temperature T_f
L_o	Sample length at reference temperature
ΔL	Total change in length of sample
ΔL_o	Change in length of sample at reference temperature
ΔL_k	Change in length of sample at temperature T_k
L_{final}	Final length of sample
$L_{initial}$	Initial length of sample
LLS	Local Load Sharing
LVDT	Linear Variable Displacement Transducer
m	Weibull shape parameter

mcp	Conductor heat capacity
MMC	Metal Matrix Composite
N	Number of experiment test
NEETRAC	National Electric Energy Testing Research and Application Center
PMC	Polymer Matrix Composite
q_c	Convection heat loss
q_r	Radiation heat loss
q_s	Solar heat gain
Q_{se}	Total heat flux
R	Conductor resistance
ROW	Right of Ways
RT	Room Temperature
S.D	Standard Deviation
SM	Storage modulus
T_a	Ambient temperature
T_c	Conductor temperature
T_f	Thin film temperature around conductor
T_{final}	Final temperature of sample
T_g	Glass transition temperature
$T_{G\inf}$	Glass transition temperature of fully cured epoxy network
T_H	Conductor temperature at resistance $R(T_H)$

$T_{initial}$	Initial temperature of sample
T_k	Temperature at every measured point k
T_L	Conductor temperature at resistance $R(T_L)$
TMA	Thermal Mechanical Analysis
T_o	Reference temperature
t_r	Time to relaxation
t_s	Time to failure
v_w	Wind speed
Z_c	Azimuth angle of the sun
Z_l	Azimuth angle of transmission line
σ_s	Tensile strength of carbon conductor core at temperature T
σ_{To}	Tensile strength of carbon conductor core at temperature T_o
ν	Poisson's ratio
σ_g	Tensile strength of CFRP in glassy region
σ	Tensile strength of CFRP at temperature T and time to failure t_s
α	Coefficient of thermal expansion
α_{avg}	Average coefficient of thermal expansion
α_{avgi}	Average coefficient of thermal expansion of sample for particular test
α_{mean_avg}	The mean of average coefficients of thermal expansion of sample
ρ_f	Air density at temperature T_f

μ_f	Dynamic viscosity of air at temperature T_f
ϕ	Angle between the wind direction and conductor axis
β	Angle between the wind direction and perpendicular to the conductor axis
α_{ab}	Solar absorptivity
θ	Angle of incidence
ε	Emissivity

CHAPTER 1

INTRODUCTION

1.1 Background

The electric power demand is increasing with each year. It is estimated that the growth in electric power demand will be approximately 28% by 2040 in the United States [1]. The current growth rate of electricity demand is 0.7% with an average growth of 0.9% per year [1]. The study findings given in reference [2] indicate that the utility industry will need new investments in generation infrastructure, with investment costs of billions of dollars, to supply the increasing demand. In order to meet the increasing power demand, significant investments in transmission and distribution infrastructure are necessary to keep pace with the increase in generation [2], [3]. The growth rate of electric power consumption in the mountain states of the U.S is highest at 1.52% per year [4]. Historically investment in transmission and distribution has been neglected for decades [3], [5]. This has led to congestion in the grid. The congestion in the grid can be attributed to other factors such as deregulation of the power industry, changing thermal limitations of transmission lines in existing right of ways (ROWs) and aging of power equipments [5]-[7]. Renewable portfolio standards, on the other hand, impose obligations on the utility industry to increase the penetration of renewable resource generation in the grid [8]. Renewable generation sites such as wind and solar tend to be far away from the load centers [3]. In order to transfer the generated power to customers, increase of present transmission capacity is required. However, as mentioned earlier, deterioration in transmission investment has occurred. To put things in perspective, transmission and

distribution investment in the US has decreased by 44% in 1980-99 [3]. The nation's grid infrastructure is also degrading and aging. This has lead to brownouts and blackouts due to sag violations of traditional transmission conductors trying to supply increased power demand, especially during the summer months [5]. In brownouts, the system voltage drops for an amount of time in order to manage load during emergency. There are three solutions to overcome the problem of achieving increased power flow in the grid to meet the electricity demand [9]. These are –

1. Line compaction – As the name suggests, the distance between the phases of the transmission line are reduced. This has the effect of reducing the line reactance. Reduction in line reactance increases the power transfer capability and thus reduces congestion in the line [9].
2. Six phase transmission system – The six phase transmission system has the advantage of requiring lesser voltage level for the same amount of power transmission as compared to three phase power system [9]. Studies indicate that the ROWs requirement is also less due to smaller tower structures [9].
3. High Temperature Low Sag (HTLS) conductors – As the name suggests, these conductors have superior sag-temperature characteristics. HTLS conductors are generally used in thermally limited lines because replacing lines, which are limited by system stability limits, with HTLS conductors will not alleviate the problem [9], [10]. HTLS conductors are expected to operate at temperatures well above 100°C continuously with emergency temperatures of 200°C - 240°C [11], [12]. The power transfer capability can thus be increased in circuits containing HTLS conductors. The major advantage of increasing the power flow with the

help of this method is that construction of new supporting structures and development of new ROWs are not required [10].

Traditionally, the power system industry has responded to increase in power demand by increasing the system voltage levels [13], [14]. American Electric Power developed 765 kV Extra High Voltage (EHV) in 1960s to meet the increasing power demand [14]. Building new transmission lines entails acquiring and developing new ROWs by utility companies. This is a complex process, which involves easement contract and maintenance of ROWs [15], [16]. The use of HTLS conductors to increase the power transfer capability to meet the rising power demand ensures reduction in constructing new tower structures and development of new ROWs, since existing ROWs and supporting tower structures can be utilized for replacement of the traditional conductors by HTLS conductors [10], [17]. Thus, for thermally limited lines, one of the most attractive investments in transmission to increase the power flow is the use of HTLS conductors. Comparatively, little research has been conducted to study the capability of HTLS conductors to handle large current flow at elevated temperatures. This thesis focuses on the mechanical characterization of HTLS conductors with temperature. HTLS conductors consisting of metal matrix core (MMC) and carbon composite core or polymer matrix core (PMC) has been considered in this study. The following sections present the thesis objectives and previous relevant research on HTLS conductors and its constituent materials.

1.2 Thesis objectives

The main objective of the project is to quantify the loss of mechanical strength of HTLS conductors with temperature. High temperatures cause annealing of aluminum

conductor wires and can cause degradation of the conductor core [17], [18]. Apart from the loss in strength of conductor, sagging of the line occurs at elevated temperatures. Sag dictates the power transfer capability of thermally limited transmission lines. The sag is dependent on the temperature of the line, which in turn depends on the amount of current flowing through the line [5]. Traditional conductors like Aluminum Conductor Steel Reinforced (ACSR) have a maximum operating temperature of 100°C [19]. HTLS conductors are designed to operate at temperatures up to 250°C without significant loss of strength. The HTLS conductors studied in this thesis are Aluminum Conductor Composite Reinforced (ACCR) and Aluminum Conductor Composite Core (ACCC). ACCR is manufactured by 3M company and ACCC is manufactured by Composite Technologies Corporation (CTC) Global. There are other manufacturers of ACCC such as Midal Cables Ltd and Alcan Cable. ACCR have metal matrix core (MMC) and ACCC have carbon composite core/ polymer matrix core (PMC). In this thesis, carbon composite core and polymer matrix core (PMC) has been used interchangeably. The coefficient of thermal expansion of the HTLS conductor MMC and PMC cores are significantly less than that of ACSR steel cores [11], [12], [20]. HTLS conductors sag less than equivalent ACSR conductors due to low coefficient of thermal expansion.

Another important aspect that has been studied closely in this thesis is the temperature rise of HTLS conductors during fault currents. This study was performed using the guidelines outlined in IEEE 738-2006 standard [21]. C++ programs were written to simulate the temperature rise in metal matrix core and carbon composite core based HTLS conductors during fault currents. The effects on the HTLS conductors were

deduced from the results of the simulation. The objectives of the thesis can be summarized below,

1. Obtain and quantify mechanical strength variation of HTLS conductors with temperature.
2. Investigate the coefficient of thermal expansion of the HTLS conductor core.
3. Study the temperature rise in the HTLS conductor due to fault currents and obtain current temperature relationships.

1.3 HTLS conductors and relevant research reviews

The power transfer capability can be increased with the help of HTLS conductors in thermally limited lines. Traditionally heterogeneous conductors like ACSR were introduced to improve sag-temperature characteristics and thermal ratings over homogenous conductors like All Aluminum Conductor (AAC) and All Aluminum Alloy Conductor (AAAC) [22]. However, over the years, electric power demand has increased but the investment in new transmission lines have not kept pace. Thus, as mentioned before, congestion in the grid has increased. Presently, the trends have shifted to large investment in new transmission infrastructure. This includes introduction of HTLS conductors for existing transmission lines that are thermally limited [10]. HTLS conductors make it possible to have a power flow increase of 2-3 times over traditional ACSR conductors in existing transmission corridors. For example, DRAKE ACSR have a current carrying capacity of 1000 A at 100°C, whereas equivalent carbon composite based HTLS conductor have a current carrying capacity of over 1600 A at 180°C [21]. This translates into a power flow increase by at least a factor of 2.5 in lines replaced by carbon composite based HTLS conductors.

ACSR conductor, which is widely used for transmission lines, is a concentrically stranded conductor. It is consists of a relatively non-conducting steel core. The steel core is galvanized to prevent corrosion. The aluminum wires which covers the steel core is a hard drawn 1350 aluminum wire with H19 temper [22]. The maximum operating temperature of ACSR conductors is 100°C [19]. Above this temperature, annealing of the aluminum wires takes place which results in rapid degradation of tensile strength of the conductor. Morgan [18] and Harvey [23] have investigated the loss of tensile strength of overhead transmission conductors due to annealing. Both provide empirical formulas to calculate the loss of strength for ACSR conductors with temperature and time.

Due to increase in power demand, aging of grid infrastructure and thermal limitations, it is difficult to ramp up power flow through existing ACSR lines. This has lead to the introduction of conductors that have better sag-temperature characteristics and higher ampacity [13]. These conductors are known as HTLS conductors. Recent introduction of HTLS conductors include ACCC and ACCR. Other types of HTLS conductors are -

1. ACSS – Aluminum Conductor Steel Supported
2. GTACSR – Gap type Aluminum Conductor Steel Reinforced
3. ZTACIR – Zirconium Type Aluminum Conductor Invar Steel Reinforced

This thesis focuses on HTLS conductors with metal matrix core and carbon composite cores. In particular, samples from ACCR and ACCC have been used for the study.

The carbon composite core or PMC based HTLS conductor consists of glass-carbon fiber/ epoxy matrix core. The core is organic in nature due to the epoxy matrix.

The glass fiber/epoxy shell encases the carbon fiber/epoxy section. The function of the glass fiber/ epoxy shell is to isolate electrically the conducting carbon fiber/epoxy section of the core [6]. Thus, the glass fiber/epoxy acts like a dielectric medium and prevents galvanic corrosion between carbon fibers and aluminum wires. The core is not stranded; it is a single piece of rod running through the entire length of the conductor. The conductor wires, which surrounds the core, are fully annealed 1350 – O tempered aluminum [5], [11]. The conductor core is produced by pultrusion process [24]. The aluminum wires are arranged in trapezoidal configuration. The advantages of HTLS conductor with carbon composite cores are manifold. It offers large cross section area for the aluminum conductors, which consequently increases the ampacity compared to equivalent ACSR, a high strength to weight ratio, superior sag-temperature characteristics, extremely low coefficient of thermal expansion of the core and high tensile strength [5]. Fig 1.1 shows the picture of ACCC, which is a carbon composite core based HTLS conductor.

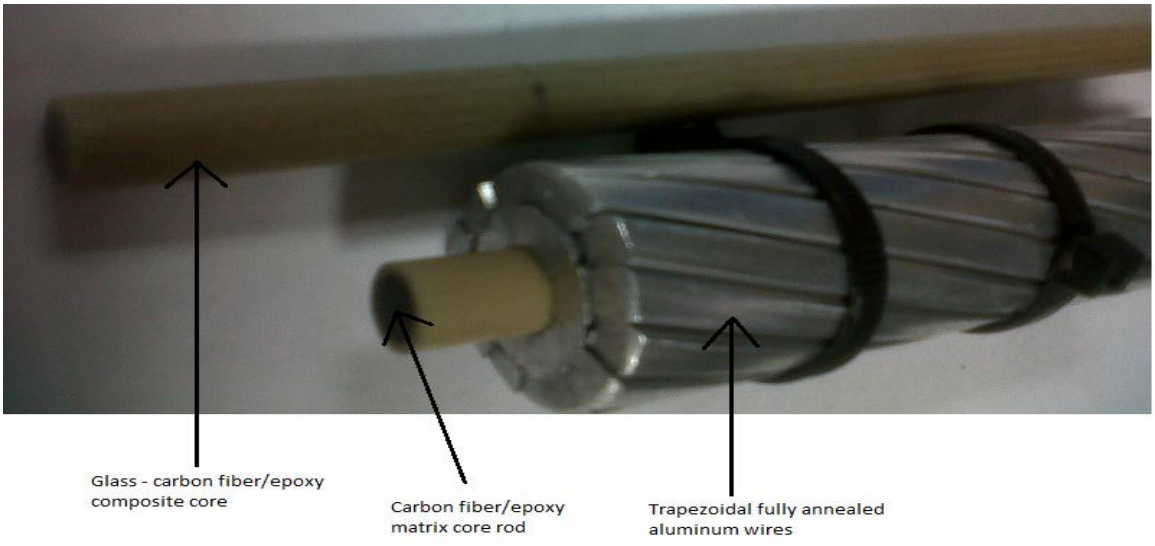

Fig 1.1 Photograph of Aluminum Conductor Composite Core (ACCC)

The metal matrix core (MMC) based HTLS conductor is designed to have significant property improvements over traditional ACSR conductors. These conductors have alumina fiber/aluminum matrix strands in the core. The aluminum matrix contains high purity aluminum. The alumina fibers are micrometer sized and are embedded in the aluminum matrix. The core consists of several alumina fiber/aluminum matrix strands and it is surrounded by high temperature aluminum –zirconium alloy wires. These wires can resist annealing up to temperatures of 210℃ [25]. The aluminum zirconium wires provide added strength to the conductor and can be arranged in round wire or trapezoidal configurations [25]. The key features of this conductor are high tensile strength, high conductivity and high strength to weight ratio [25]. Compared to ACSR, it can retain its tensile strength at temperatures above 100℃ and sags less at high temperature due to low coefficient of thermal expansion [10], [12], [18], [20], [23], [25]. Fig 1.2 shows the picture of ACCR, which is a MMC based HTLS conductor.

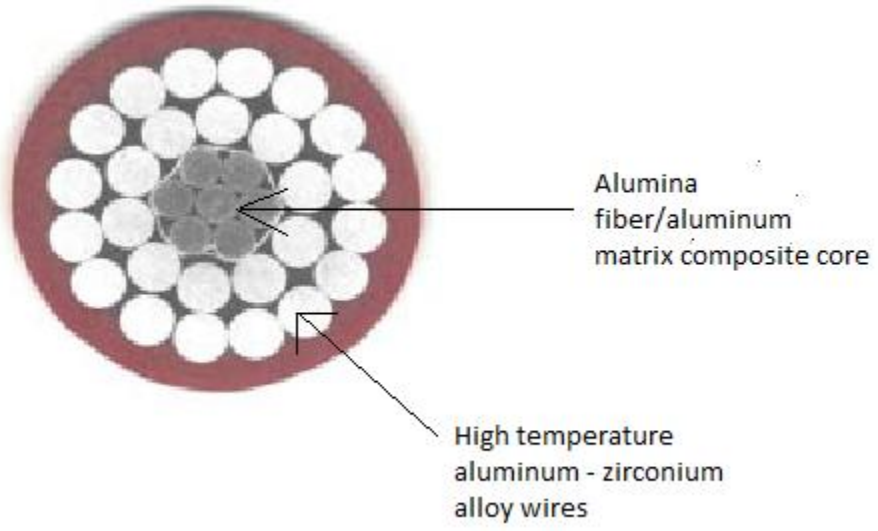

Fig 1.2 Diagram of Aluminum conductor composite reinforced (ACCR) [12]

HTLS conductor technology is comparatively new. The utilities do not have enough confidence in the performance of these conductors. To familiarize with the operation and handling of HTLS conductors like ACCC and ACCR, various field trials of the conductors were undertaken by Arizona Public Service, San Diego Gas & Electric and other utilities [10], [26]. Arizona Public Service have tested 1020 kcmil ACCC DRAKE equivalent at 69 kV transmission system in Phoenix, Arizona. The conductors were installed between four spans in 2005 with a total length of 956 ft. San Diego Gas & Electric have field-tested ACCR conductor of 795 kcmil which replaced ACSR conductor of 636 kcmil in a 69 kV transmission circuit in Oceanside, California. The conductors covered four spans of total length of 902 ft. The conductors were installed in 2005. These field tests monitored the conductor loading, sag -tension, corona and electric and magnetic fields continuously. According to the results of these field tests, the conductors performed as expected with all the parameters normal. In addition to these field tests, 3M company have conducted their own outdoor tests on ACCR in Oak Ridge National Laboratory (ORNL) [27], [28]. The ACCR conductors were thermally cycled and exposed to various weather conditions. The conductors were then tested for residual tensile strength and stress-strain behavior. The results indicated that the conductors did not show any appreciable loss of tensile strength from clean conductor samples. Apart from field trails, manufacturing companies for ACCC and ACCR have tested the conductors for sag performance, fatigue, creep, aileron vibrations and stress strain relationships [12], [29]. Utilities and transmission operators around the world have successfully deployed ACCC and ACCR conductors commercially in various

environments like heavy ice and marine installation, densely populated areas, etc [29], [30].

Coefficient of thermal expansion of a transmission line is an important parameter. It indirectly determines the sag of a conductor, thus dictating thermal rating of the line. Various researches have been conducted to determine the coefficient of thermal expansion of the constituent materials of HTLS conductor. The coefficient of thermal expansion for carbon fibers and carbon fiber/epoxy composites has been extensively and experimentally determined in references [31]-[33]. The coefficient of thermal expansion for carbon fiber/epoxy composite range from $-0.6\times10^{-6}/K$ to $-0.001\times10^{-6}/K$ in the direction of the carbon fibers in the composite. Burks, Armentrout and Kumosa [34] used the axial and transverse coefficient of thermal expansion of the carbon composite core in ACCC to develop finite element models to predict the axial and transverse stresses in the core due to thermal mismatch between the carbon fibers, glass fibers and epoxy matrix. National Electric Energy Testing Research and Applications Center (NEETRAC) performed coefficient of thermal expansion measurements for ACCR and it was noted that the difference or mismatch in thermal expansion characteristics between the metal matrix core and the aluminum conductor wires caused complex behavior of the conductor [35]. Thermal kneepoint of a conductor plays an important role in determining the thermal expansion of the conductor [36]. Below the thermal kneepoint, the coefficient of thermal expansion of a conductor is due to both aluminum wires and the core. Above the thermal kneepoint, the core carries the load almost entirely and consequently the coefficient of thermal expansion of the conductor reflects that of the core. Since HTLS conductors cores of ACCR and ACCC have very low coefficient of thermal expansion as

compared to ACSR, HTLS conductors sag less at high temperatures than ACSR. In fact, above the thermal kneepoint, ACCC shows the unique feature of almost flat sag temperature characteristics [37]. The thermal kneepoint for HTLS conductors like ACCR and ACCC occurs at lower temperatures than that of ACSR [10].

Bosze [38] showed that there is a correlation between the loss of tensile strength of carbon composite core of HTLS conductor and loss of storage modulus of the carbon-fiber/epoxy section of the core. Dynamic Mechanical Analysis (DMA) was used to determine the loss of storage modulus with temperature. The normalized curve of loss in storage modulus is equivalent to the normalized curve of loss in tensile strength. The correlation is given by equation 1.1,

$$\sigma_s(T) = \sigma_{To}\left[\frac{E'_T}{E'_{To}}\right] \tag{1.1}$$

Where,

σ_s is the tensile strength at temperature T

σ_{To} is the tensile strength at temperature T_o

E'_T is the storage modulus at temperature T

E'_{To} is the storage modulus at temperature T_o

In DMA, a sinusoidal stress force is applied to visco-elastic material such as carbon fiber/epoxy composite [39], [40]. The strain response of the material is also sinusoidal but lags the stress by an angle. This phase difference is due the energy absorbed in the material without performing any deformation. This is analogous to a response of an R-L circuit to a sinusoidal voltage. This leads to the concept of complex modulus in viscoelastic materials. The complex modulus is given by equation (1.2),

$$E = E^{'} + iE^{''} \tag{1.2}$$

Where,

E is the complex modulus,

$E^{'}$ is the storage modulus,

$E^{''}$ is the loss modulus.

The storage modulus is related to the shear modulus by equation (1.3),

$$E^{'} = 2G(1+\upsilon) \tag{1.3}$$

Where,

G is the shear modulus,

υ is the Poisson's ratio.

Mathematically, the relationship of between shear modulus and tensile strength of a carbon fiber reinforced plastic (CFRP) is given by equation (1.4) [41],

$$\frac{\sigma(t_s,T)}{\sigma_g} = \left(\frac{G(t_r,T)}{G_g}\right)^{\left(\frac{1}{2m}\right)} \tag{1.4}$$

Where,

σ_g is the tensile strength at the glassy region,

σ is the tensile strength at temperature T and time to failure t_s.

G_g is the shear modulus at the glassy region,

G is the shear modulus at temperature T and time to relaxation t_r.

m is the Weibull shape parameter.

Glass transition temperature (T_g) is an important property of visco-elastic material. It is the temperature at which the material changes from glass state to

amorphous state [40]. The change is associated with the loss of stiffness of the visco-elastic material. Glass transition temperature can be determined with the help of various techniques such as Differential Scanning Calorimetry (DSC), Thermal Mechanical Analysis (TMA) and DMA where DMA is considered the most sensitive technique to measure T_g [42]. There are several methods to determine glass transition temperature in DMA analysis [43]. Tan delta peak is used in the DMA of ACCC carbon core as the glass transition temperature. This method reflects the midpoint between the glassy and rubbery states of the material [43].

Rossoll [44] predicted the failure mechanism of ACCR metal matrix core under tensile load. In this research, local load sharing (LLS) mechanism and global load sharing (GLS) mechanism were applied to the failure of the conductor core. The predicted tensile strength values of the conductor core at different temperatures by the LLS mechanism were in good agreement with the experimental values. The strength of the core decreased by 4% from room temperature to 200°C. The loss of tensile strength of the core at 300°C was 10%. At 600°C, the loss of tensile strength was 30%. The melting point of the aluminum in the metal matrix is 650°C.

Thermal aging experiments on HTLS conductors provide insight on the mechanical response of the conductors to stress due to heat. Thermal aging of carbon composite cores presented in references [45]-[47] shows that the cores retain its tensile strength at room temperature. It also reveals that the glass fiber layer of the core protects the carbon fiber layer from oxidation. Thermal aging at different temperatures and lifetime modeling of aluminum zirconium alloy wires and alumina/aluminum matrix core used in ACCR were carried out by 3M company [48], [49]. The core samples were aged

at up to 500°C for a maximum of 2000 hours whereas the aluminum-zirconium alloy wire samples were aged at up to 400°C for a maximum of 1000 hours. The studies concluded that that there is statistically insignificant variation in the tensile strength of the aged core samples at room temperature and the aged samples retained their tensile strength. Lifetime modeling based on thermal aging of the aluminum-zirconium alloy wires concluded that the wires would lose 10% of its strength in 40 years when exposed continuously to 240°C.

1.4 Steady state and transient thermal ratings of overhead transmission conductors

Every overhead transmission line has a maximum operating temperature, which determines the thermal rating of the line. The thermal rating depends on the ambient weather parameters, conductor characteristics and conductivity [21], [47]. The passage of current through the conductor produces heat and along with solar radiation absorbed by the conductor balances the heat loss through convection and radiation [5], [21]. Traditionally, thermal ratings of overhead conductors are determined by assuming conservative values of ambient weather parameters such as 0.61 ft/s wind speed and high ambient temperature of 40°C [21]. The conductor characteristics include emissivity and absorptivity, which are usually taken as 0.5 [21]. CIGRE and IEEE have standardized the process of calculating the thermal ratings of overhead transmission lines [21], [50]. The latest IEEE standard for calculating the current temperature relationship of overhead bare conductors is the IEEE 738-2006 [21].

Thermal ratings indirectly provide the ampacity of the conductor. Ampacity is the maximum amount of current that a conductor can carry at the maximum allowable temperature under a certain set of weather parameters and conductor characteristics [47].

The maximum allowable temperature or the design temperature of the conductor depends on the sag and loss of tensile strength of the conductor with temperature. The thermal rating of the line depends on the aging of the line since the conductor characteristics changes with time [21]. These factors have to be taken into account when estimating the current carrying capacity of the line over its lifetime.

The steady state thermal rating of the line is calculated when the line is in thermal equilibrium. Whereas, the transient thermal rating of the line provides the rate of temperature rise to its steady state value when there is a step increase in the current flowing though the conductor. The rate of temperature rise depends on the conductor's overall heat capacity [21]. The temperature of the conductor will rise slowly if the heat capacity of the conductor is high and vice versa. In transient thermal rating calculations due to fault currents, the heat capacity of the conductor core is generally neglected for fault duration of less than 60 seconds [21]. The thermal time constant for transient thermal rating calculations depends on the ac resistance of the conductor, heat capacity and difference between the square of the final and initial current magnitudes [21].

1.5 Thesis organization

In chapter 2, thermal aging experiments of carbon composite cores are presented. The carbon fiber/epoxy samples from ACCC is used for the experiments. The physical changes of the carbon composite cores due to heat exposure are observed with the help of an optical microscope and are described in this chapter. An explanation of the observed physical changes is also given.

Chapter 3 describes the TMA experiments for obtaining the coefficient of thermal expansion of the composite conductor cores. Detailed analysis of the experimental results

is discussed. The mean and standard deviation of the thermal expansion coefficient of both metal matrix core and carbon composite core is established.

In chapter 4, DMA of carbon composite cores is presented and loss of storage modulus of the carbon core with temperature is obtained. Analysis of the loss of storage modulus of the cores is described. Percentage loss of tensile strength of the conductor core is estimated with the help of the loss of storage modulus of the carbon cores.

In chapter 5, the tensile testing of metal matrix core is described. Development of new custom grips for the tensile testing is discussed. Stress – strain relationship of the core is established from the load – displacement curve obtained from the tensile test.

Chapter 6 describes the calculation of current temperature relationships and temperature rise due to fault currents for the composite core conductors with the help of IEEE 738-2006 standard. The chapter also discusses the C++ programs written to simulate the temperature rise due to steady state currents and transient fault currents. The effect of the temperature rise due to fault currents on the structure of the composite cores has been discussed.

Chapter 7 provides the conclusion on the study of HTLS conductors with composite cores. It also presents the future work based on this present study.

CHAPTER 2

HEAT TREATMENT OF CARBON COMPOSITE CORES

This chapter describes the heat treatment or thermal ageing of carbon composite cores of HTLS conductors. The maximum continuous operating temperature for these types of HTLS conductors is 180°C, with an emergency maximum temperature of 200°C [11]. The epoxy matrix of the carbon composite core is an organic material and organic materials are susceptible to degradation at high temperatures [17], [47]. Thus, degradation of the carbon composite core may occur due to heat treatment. Heat treatment of the carbon composite cores at various temperatures was performed in order to observe the degradation of the carbon fiber/epoxy matrix section as well as the glass fiber/epoxy matrix shell of the carbon composite.

2.1 Test setup

The test setup consists of high temperature Muffle Furnace. The muffle furnace is of Barnstead/Thermolyne Corporation make [51]. These are general purpose laboratory furnace and has a temperature range of 25°C - 1700°C. The maximum ramp rate as detailed in its user manual is 100°C/min. The muffle furnace consists of abrasive heating elements made up of alumina and silica. The thermocouple is made from a precious metal. The current controller of the furnace compares the temperature in the furnace chamber with the temperature set point and provides the appropriate current to its heating elements. In case of overheating due to overcurrents, relays and circuit breakers are provided.

The temperature of the heat treatment of the samples is programmed into the furnace. Samples were kept in isothermal zones of 125°C, 175°C, 200°C, 250°C and 300°C for 24 hours each. Some samples were kept for 40 hours at 125°C. The environment inside the muffle furnace chamber were the samples were kept was air. The test setup is shown in Fig 2.1.

Fig 2.1 Muffle furnace used for the heat-treatment of the carbon composite cores

2.2 Sample description

The samples used in this experiment were sectioned out from the ACCC carbon core. The ACCC carbon core consists of concentric glass fiber/epoxy matrix shell covering the carbon fiber/epoxy matrix rod. The samples were 1-2 cm in length and had a diameter of 9.53 cm, which is the diameter of the core in DRAKE sized ACCC. Fig 2.2 shows the cross section of an untreated sample. The samples were cut from the ACCC

core rod with the help of carbide cutting tool. The difference in the coefficient of thermal expansion of the components of the core such as glass fiber/epoxy and carbon fiber epoxy can contribute to thermal stresses during thermal aging [34]. There are two types of interfaces present in the sample [34] –

1. Fiber matrix microscopic interface
2. Composite – Composite macroscopic interface (e.g. glass fiber/epoxy – carbon fiber/epoxy)

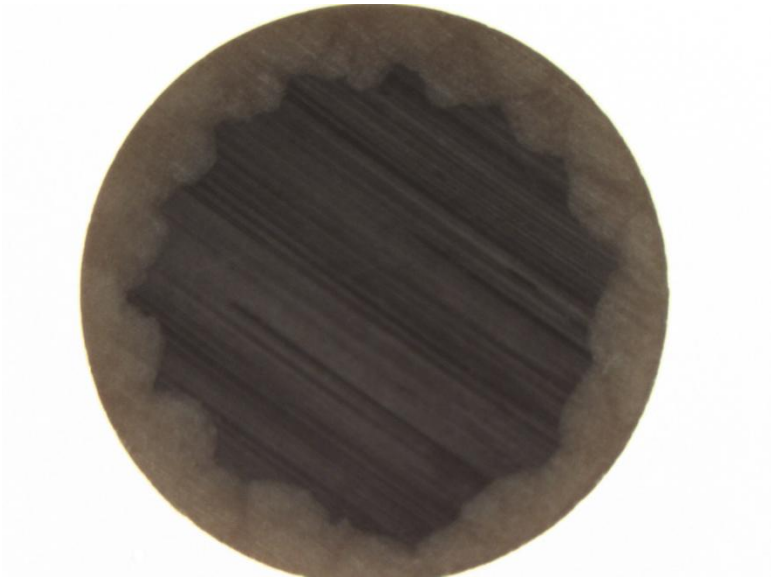

Fig 2.2 Cross section view of untreated carbon composite core

2.3 Results and discussion

The thermal aging of samples heat treated at different temperatures are shown in the Fig 2.3 – 2.7. Fig 2.3 shows the cross section of the sample heat – treated at 125℃ for 24 hours. It can be seen that there are no cracks on the cross section of the sample. Fig 2.4 shows the sample heat – treated at 150℃ for 24 hours. Radial cracks on the cross section of the sample can be seen. Fig 2.5 shows the cross section of the sample kept at

200°C for 24 hours. Similarly, Fig 2.6 and 2.7 shows the cross section of the sample for 250°C and 300°C.

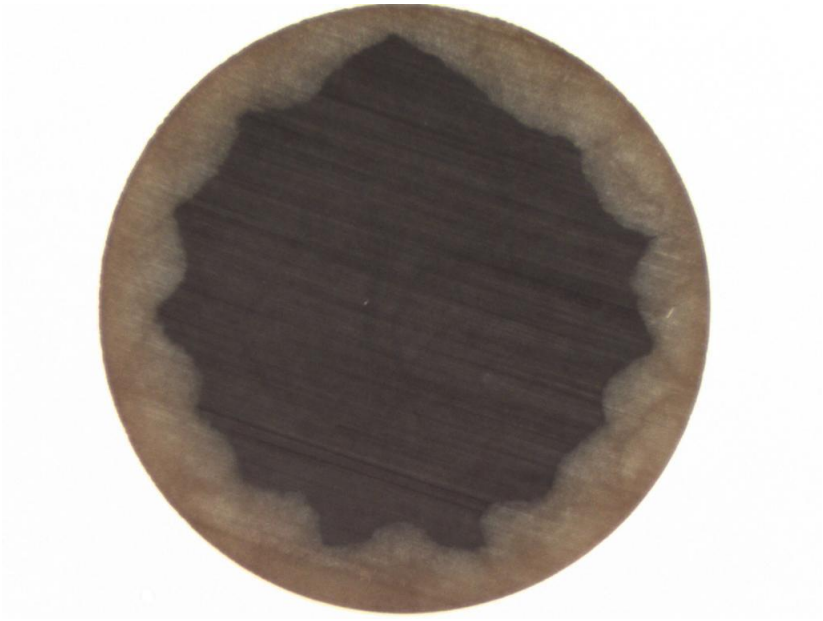

Fig 2.3 Cross section of the sample heat-treated at 125°C for 24 hours

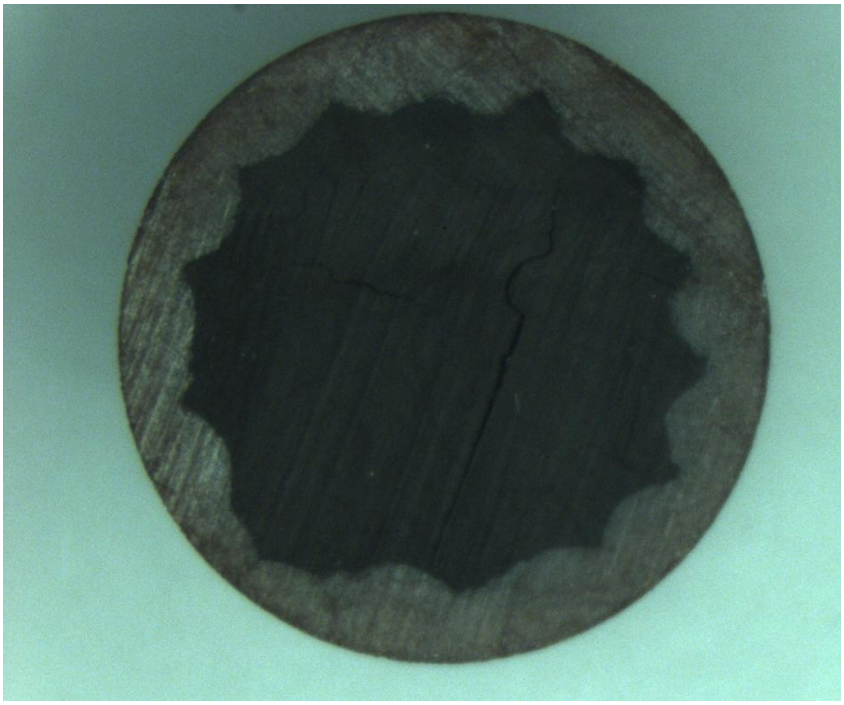

Fig 2.4 Cross section of sample heat treated at 150°C for 24 hours

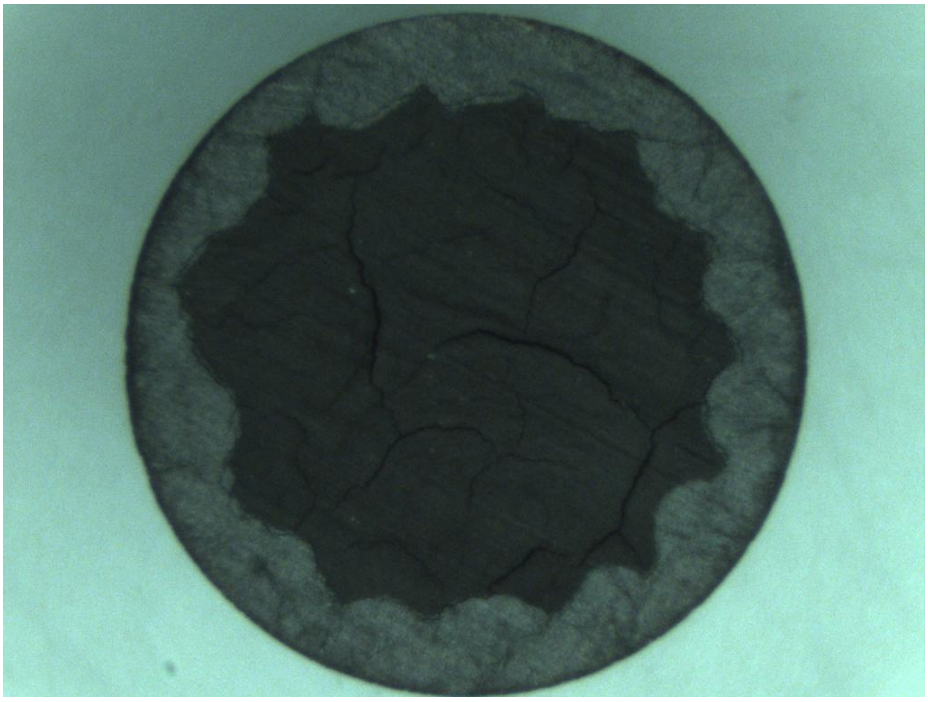

Fig 2.5 Cross section of the sample heat – treated at 200℃ for 24 hours

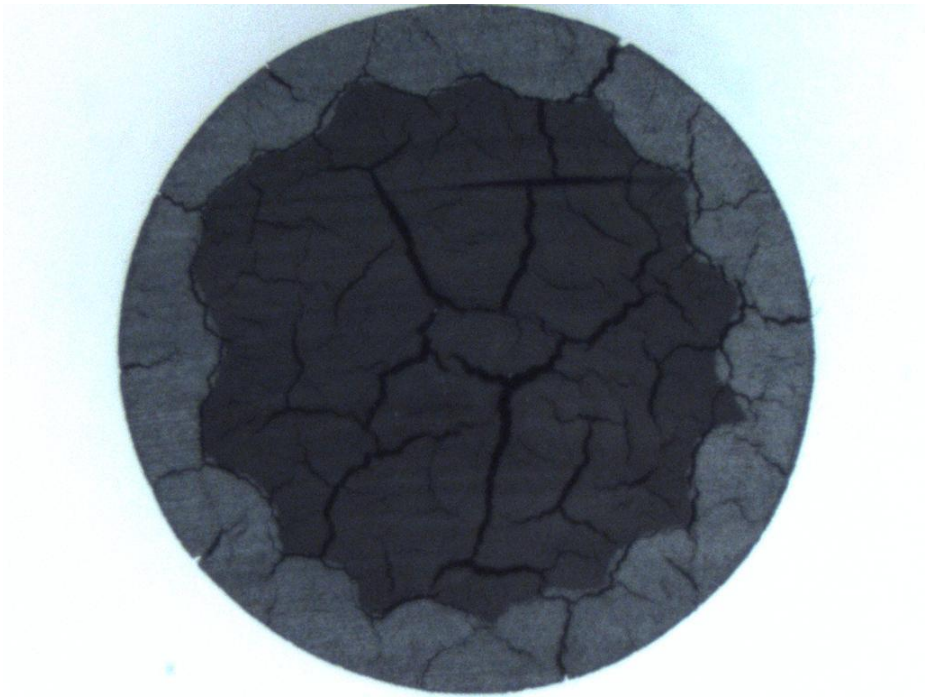

Fig 2.6 Cross section of the sample heat – treated at 250℃ for 24 hours

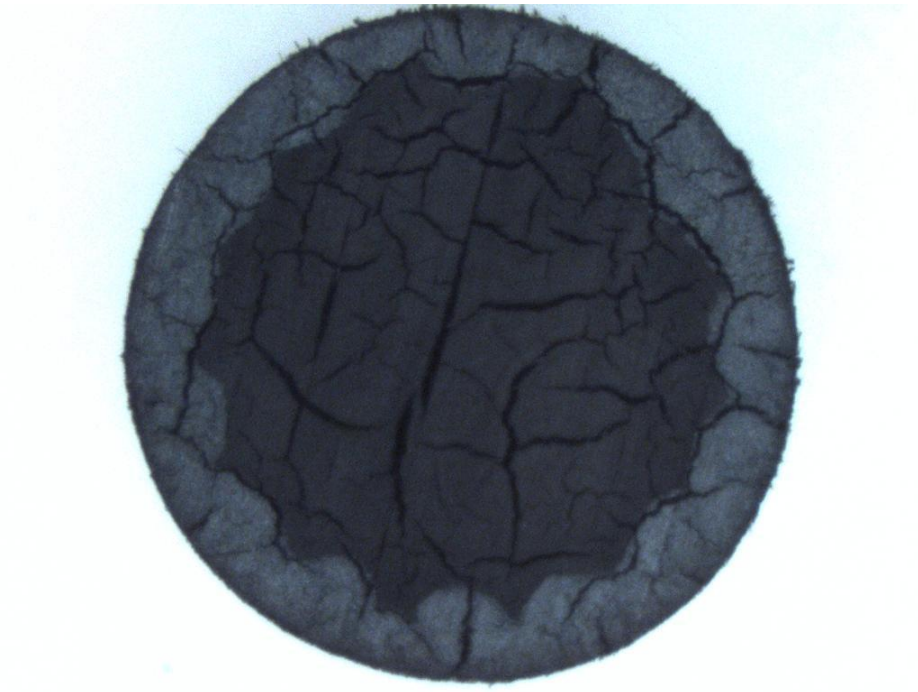

Fig 2.7 Cross section of the sample heat – treated at 300°C for 24 hours

The sample became heavily degraded due to thermal aging after 24 hours at 250°C and 300°C. Numerous radial cracks on the carbon fiber/epoxy section as well as on the glass fiber/epoxy section appeared. Some of the cracks covered the entire width of the core sample. Fig 2.8 – 2.11 shows the cracks on the macroscopic interface between the glass fiber/ epoxy and carbon fiber/epoxy of the sample kept at 150°C, 200°C, 250°C and 300°C for 24 hours respectively. The cracks on the interface increased in width with the increase in degree of heat – treatment of the sample. The cracks can be attributed to the difference in the thermal expansion coefficients of the glass fibers, carbon fibers and the epoxy matrix. At high temperatures, these materials expand differently at different rates. This causes development of thermal stress both between the fiber-matrix and glass

fiber/epoxy – carbon fiber/epoxy [34]. Thus, it leads to cracking of the epoxy matrix and the macroscopic interface.

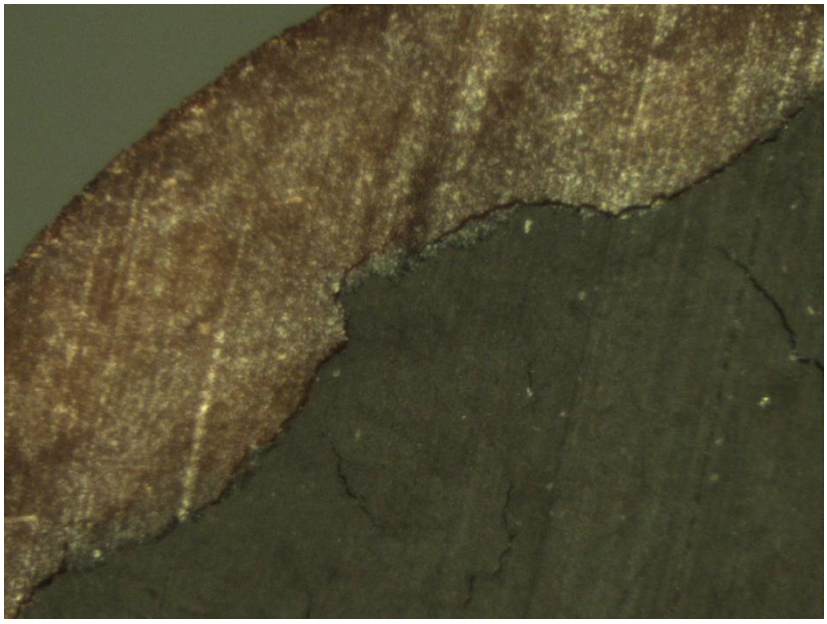

Fig 2.8 Macroscopic interface of the sample heat treated at 150℃ for 24 hours

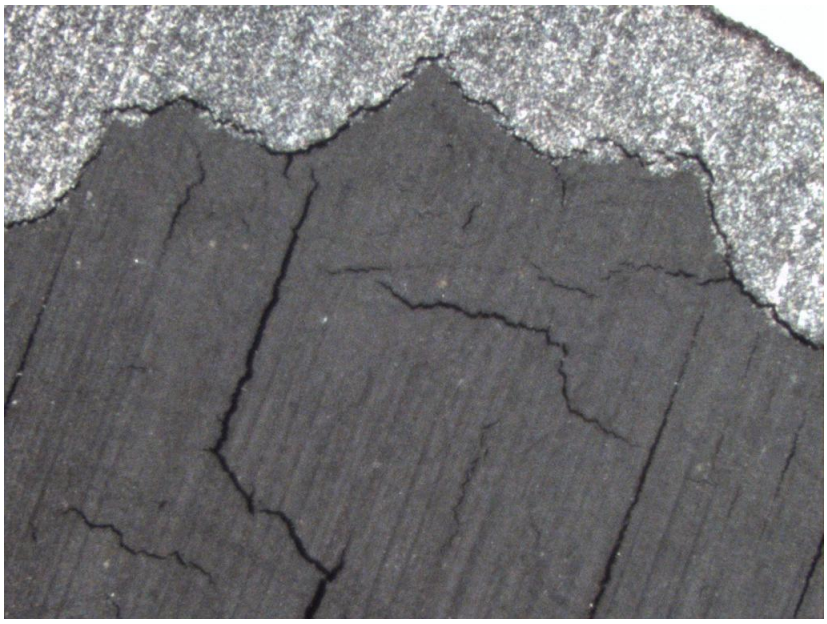

Fig 2.9 Macroscopic interface of the sample heat treated at 150℃ for 24 hours

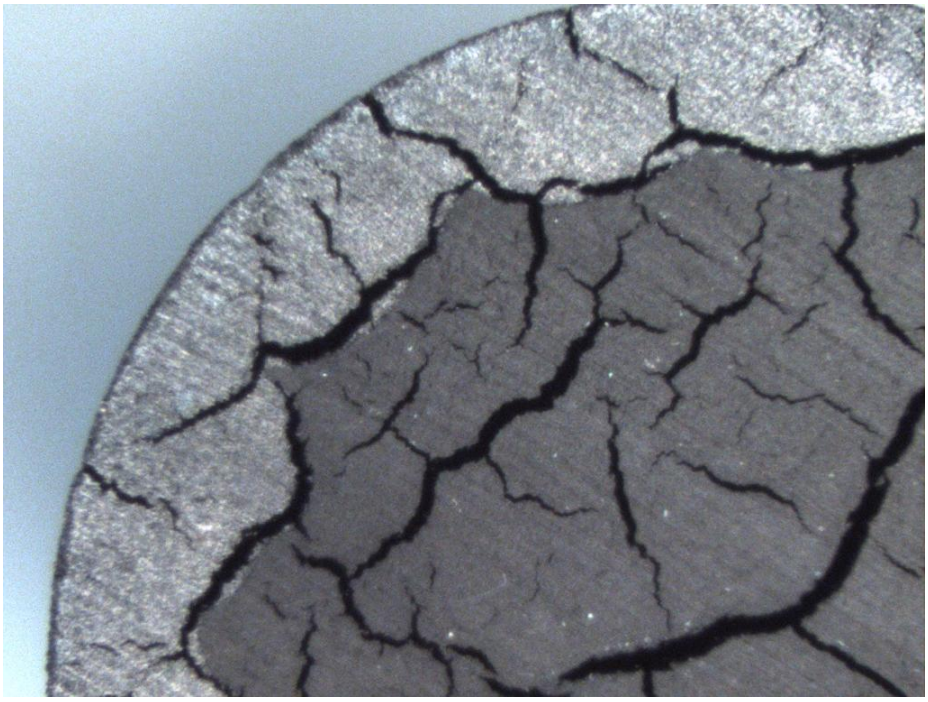

Fig 2.10 Macroscopic interface of the sample heat treated at 250℃ for 24 hours

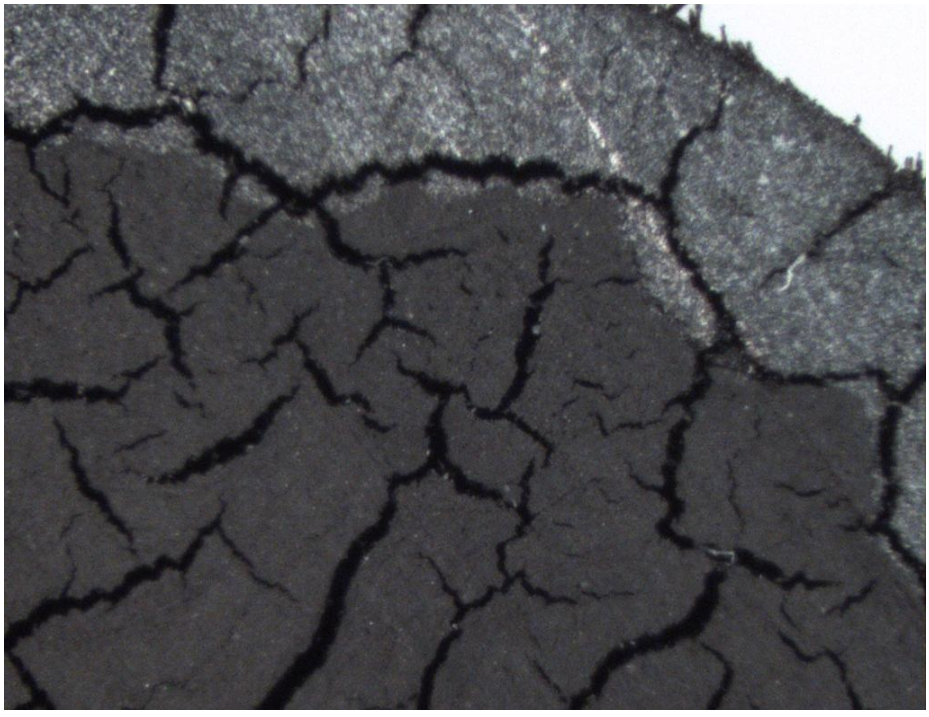

Fig 2.11 Macroscopic interface of the sample heat treated at 300℃ for 24 hours

From the heat treatment of the carbon composite cores the following points were noted –

1. ACCC conductor core samples withstood sustained temperature of 125℃ without any development of cracks on the cross section .
2. Cracks across the composite-composite interface and across carbon fiber/epoxy section were observed at 150℃ and above. These cracks are due to mismatch of coefficient of thermal expansion between glass fibers, carbon fibers and epoxy.
3. At temperatures at or above 250℃, the width of the cracks and fissures across the core and the glass fiber/epoxy – carbon fiber/epoxy increased as compared to the cracks at lower temperatures. Radial cracks from the glass fiber/epoxy –carbon fiber/epoxy boundary across the glass fiber/epoxy section were observed. This radial cracks may expose the carbon fiber/epoxy portion to the atmosphere which will cause accelerated ageing [45], [46].

CHAPTER 3

THERMAL MECHANICAL ANALYSIS OF HTLS CONDUCTOR CORES

Coefficient of thermal expansion of a material is an important mechanical property. It provides an insight on the material response to temperature exposures. The sag of a transmission conductor is dependent on its coefficient of thermal expansion [20]. At the thermal kneepoint, most of the load on the conductor shifts to its core and thus the core controls the expansion of the conductor after the kneepoint [10], [36], [37]. HTLS conductor cores consist of multiple components such as carbon fiber in epoxy matrix for composite cores and alumina fibers in aluminum matrix. The mismatch of coefficient of thermal expansion between these materials can create micro and meso stresses [34]. In this chapter, thermal mechanical analysis (TMA) on carbon composite and metal matrix cores to obtain the respective coefficient of thermal expansions has been addressed. The results obtained from TMA of HTLS cores were analyzed to get the average coefficient of thermal expansion of the cores in the temperature range of room temperature - 300°C.

3.1 Thermal mechanical analysis

Thermal mechanical analysis detects dimensional changes in a material in response to change in temperature. Coefficient of thermal expansion can be calculated from the dimensional changes such as change in length of the material. In case of the carbon composite core and metal matrix cores of HTLS conductors, coefficient of thermal expansion in the longitudinal direction is of primary concern. The TMA system calculates thermal expansion coefficient is calculated by with the help of the following equation,

$$\alpha(k) = \frac{1}{L_o} * \frac{\Delta L_k - \Delta L_o}{T_k - T_0} \qquad \text{(k = 1..n)} \qquad (3.1)$$

Where,

α is the coefficient of thermal expansion of the sample,

L_o is the sample length at reference temperature,

ΔL_o is the change in length at reference temperature,

ΔL_k is the change in length at temperature T_k,

T_o is the reference temperature

The TMA system gathers the data points corresponding to α_k for every measured point k. An important consequence of equation (3.1) is TMA system can track variation in coefficient of thermal expansion of a material with temperature. The average coefficient of thermal expansion (α_{avg}) of a material in a certain temperature range is given by the following equation,

$$\alpha_{avg} = \frac{L_{final} - L_{initial}}{L_{initial} * (T_{final} - T_{initial})} \qquad (3.2)$$

Where,

L_{final} is the final length of the material,

$L_{initial}$ is the initial length of the material,

T_{final} is the final temperature of the material,

$T_{initial}$ is the reference temperature

The software section of the TMA system applies signal correction procedures after the collection of data from the sample material under study. The three important signal correction procedures are [52] –

1. Zero correction – In this type of correction, the difference between the expansion of the piston and the sample holder is subtracted from the expansion curve of the sample. The curve signifying the difference between the expansion of the piston and the sample holder is called the zero curve.
2. Piston correction – The piston correction determines the change in length of the piston during the test and compensates this elongation by applying the coefficient of thermal expansion of the piston to the data curve to get an accurate expansion curve of the sample.
3. X-axis smoothening – This helps in smoothening the data curve over the investigated temperature range.

The accuracy of TMA measurements decreases when the coefficient of thermal expansion of the sample is much lower than the coefficient of thermal expansion of the sample holder [52]. In order to make the measurements more accurate, the sample holder should have a low coefficient of thermal expansion and the ramp rate of the temperature used in such tests should be limited to 2-5 K/min [52].

3.2 Test details

Linseis TMA/DMA L77 system was used to perform thermal mechanical analysis of the carbon composite core and the metal matrix core. Fig 3.1 shows the Linseis TMA/DMA L77 system. It consists of three parts in the hardware design [53]. The upper part of the system houses the LVDT sensor, its control circuits, amplifier, thermocouples

and the thermostat. The measuring head, which contains the piston and the sample holder, is connected to the LVDT sensor. The expansion of the sample causes the piston to move and this motion is converted into electrical signal by the LVDT. The control circuits control the linear motor that applies static or dynamic force on the sample. The system provides a cylindrical furnace, which can completely cover the glass tube housing the sample holder and piston to provide uniform heating. The thermostat controls the temperature. The whole system is interfaced with a PC with MS-Windows running Linseis data acquisition and evaluation software. TMA/DMA L77 is very sensitive to vibrations, which can distort the data signals. In order to overcome this problem to a certain extent, the legs of the machine are kept on a material, which can absorb those materials.

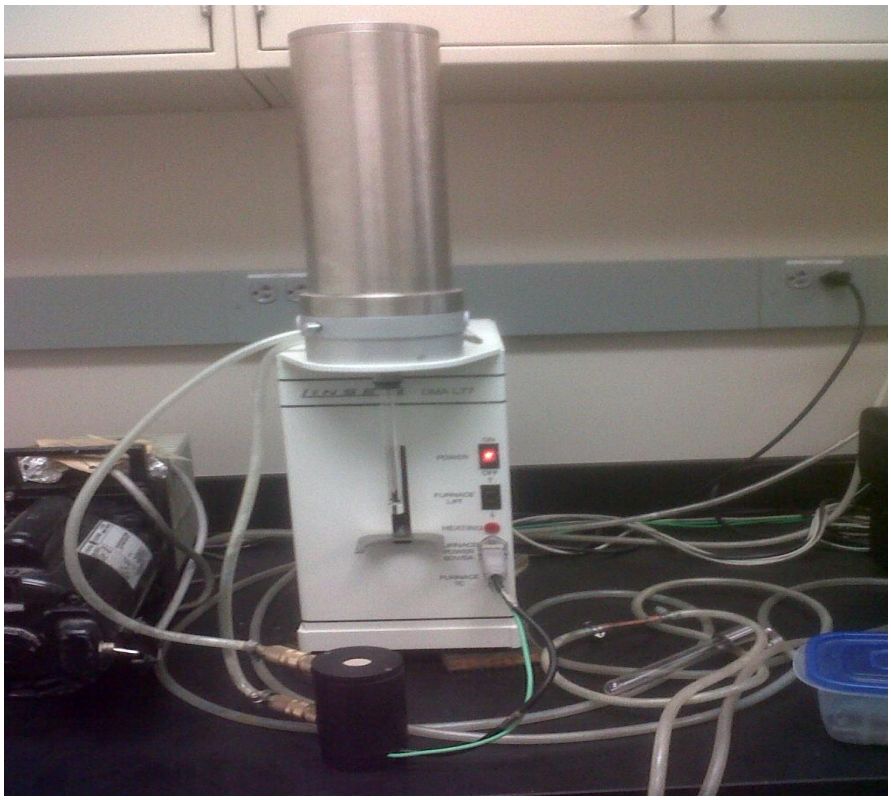

Fig 3.1 Thermal mechanical analysis (TMA) test system

Linseis data analysis software consists of three sections [53] –

1. Data acquisition section – In this section, the system acquires the dimensional change data from the TMA tests and stores it in the memory. The system also records the information about the sample and initial test conditions in this section.
2. Evaluation section – The data acquired from the system is analyzed and evaluated. This section also performs corrections on the data, if needed. Various parameters like coefficient of thermal expansion, relative and absolute change in length of the sample are calculated from the acquired data.
3. Programming section – This section is concerned with the programming of the number of temperature cycles, its ramp rate and dwell time for the TMA tests.

The following Table 3.1 lists out the test details for the evaluation of the coefficient of thermal expansion of the carbon composite core and metal matrix core of HTLS conductors.

Table 3.1
Test details for thermal mechanical analysis of the HTLS conductors

Type of core samples	Sample length (mm)	Sample diameter (mm)	No. of tests	Temperature range (°C)	Temperature ramp rate (°C/min)
ACCR	10.1	2.5	6	RT-300	5
ACCC	9.89	7.0	5	RT-300	5

Six tests were performed on ACCR metal matrix core sample and five tests were performed on ACCC carbon composite core sample. The length of the metal matrix core sample was 10.1 mm and the length of carbon composite core sample was 9.89 mm. The

temperature was ramped from ambient to 300°C and a temperature ramp rate of 5°C/min was chosen.

3.3 Sample description

The samples used in the experiments were carbon fiber/epoxy matrix and alumina fiber/ aluminum matrix cylindrical rods with smooth flat surface at the top and bottom. A smooth surface profile is important because the piston tip contacts the sample on the top and an uneven surface might cause the piston tip to slip introducing error in the signal for change of length of the sample. The carbon fiber/epoxy matrix rod was obtained from the core of ACCC after stripping off the outer glass fiber/epoxy matrix shell. The alumina fiber/aluminum matrix rod was sectioned out from ACCR core.

3.4 Experimental procedure

Thermal mechanical analysis is a non-destructive testing method. The samples do not require special preparation for the testing. The following lists out the procedure undertaken to perform CTE tests for ACCR and ACCC core samples –

1. The sample was mounted on the sample holder and the tip of the piston, connected to the LVDT, was made to touch the sample on its flat surface.
2. A protective outer glass tube was used to cover the assembly.
3. The furnace was then introduced to cover the sample.
4. Initial test conditions were entered in the Linseis TMA/DMA L77 software. A static force of 0 mN was chosen in order to obtain the thermal expansion data. The temperature ramp rate for the tests was 5°C/min.
5. The temperature was ramped from ambient to 300 °C

6. Once the software had gathered the data for the thermal expansion of the sample, zero measurement correction and piston correction were applied to the acquired signal in order to take care of the thermal expansion of the piston and the sample holder.
7. The resultant thermal expansion data were then analyzed to obtain the mean of the coefficient of thermal expansion from the tests.

3.5 Results

The Linseis data analysis software captured the thermal expansion data from the experiments for ambient - 300°C. Fig 3.2 shows the result from the thermal expansion tests on ACCR core sample. It can be seen that the change in length with temperature over the range of ambient - 300°C for ACCR core sample was approximately 16 μm. Correspondingly, the coefficient of thermal expansion of the samples increased from approximately $5\times10^{-6}/K$ to $6\times10^{-6}/K$ with temperature. The sudden variations in the curve for change in length and coefficient of thermal expansion with temperature observed in few tests were due to noise in the data signals introduced by stray vibrations.

Fig 3.3 shows the results obtained from the thermal expansion tests on the carbon fiber/epoxy part of ACCC core sample. The tests for ACCC carbon core show that the final change in length of the sample with temperature was -2.5μm. Consequently, the coefficient of thermal expansion of the ACCC core sample decrease from $0.5\times10^{-6}/K$ at initial temperature to $-0.5\times10^{-6}/K$ at final temperature. The coefficient of thermal expansion of the carbon fiber/epoxy sample becomes negative since the thermal expansion coefficient of the constituent carbon fibers is negative and it dominates the mechanical properties in the axial direction.

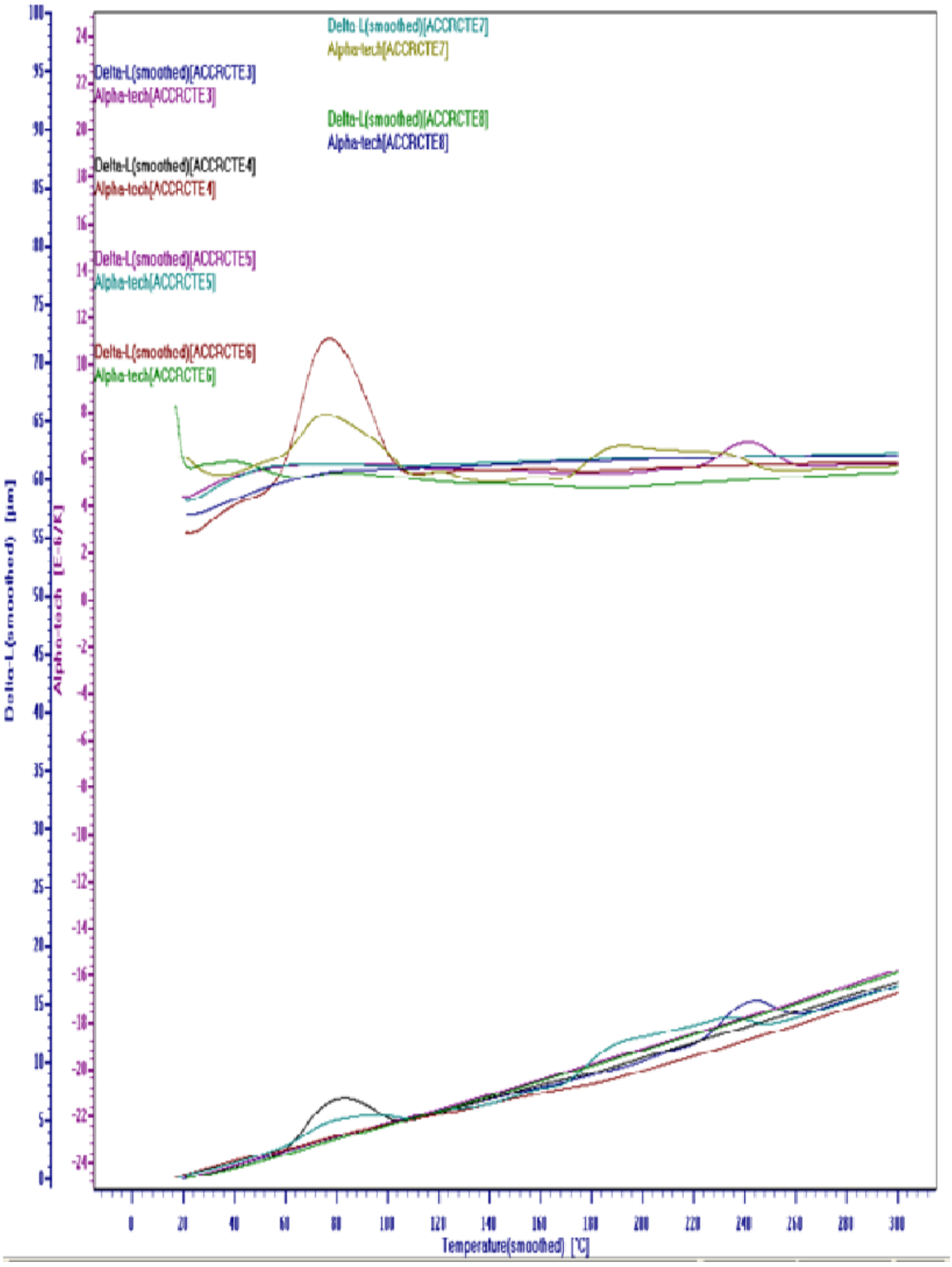

Fig 3.2 Comparison of change in length and coefficient of thermal expansion for ACCR core samples

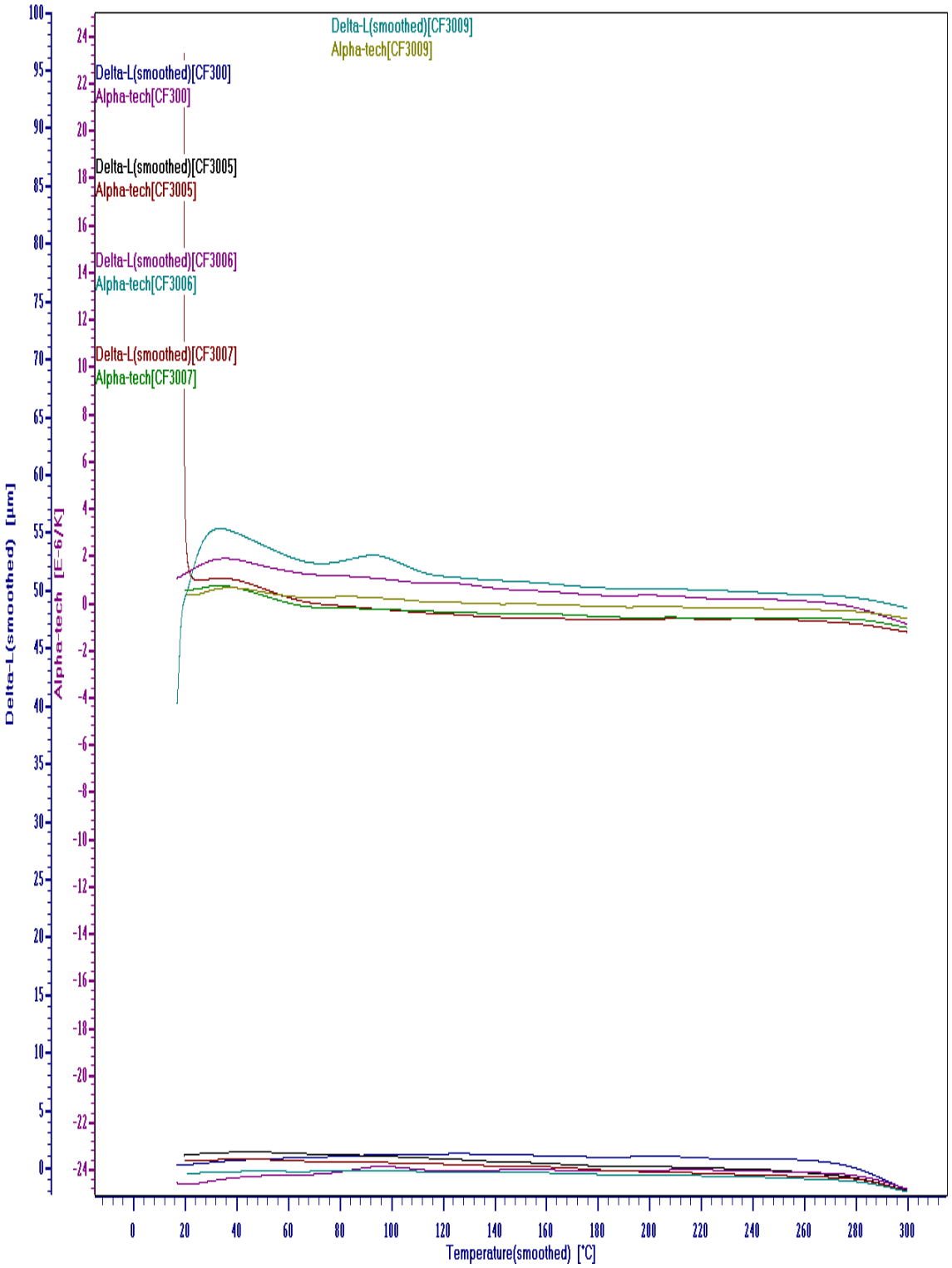

Fig 3.3 Comparison of change in length and coefficient of thermal expansion for ACCC core samples

3.6 Analysis of TMA test results

The data analysis section of the TMA software was employed to analyze the coefficient of thermal expansion curves obtained in the tests for ACCR and ACCC core samples. The mean, maximum and minimum of the coefficient of thermal expansion curves obtained from different tests on ACCR core sample is given in Fig 3.4.

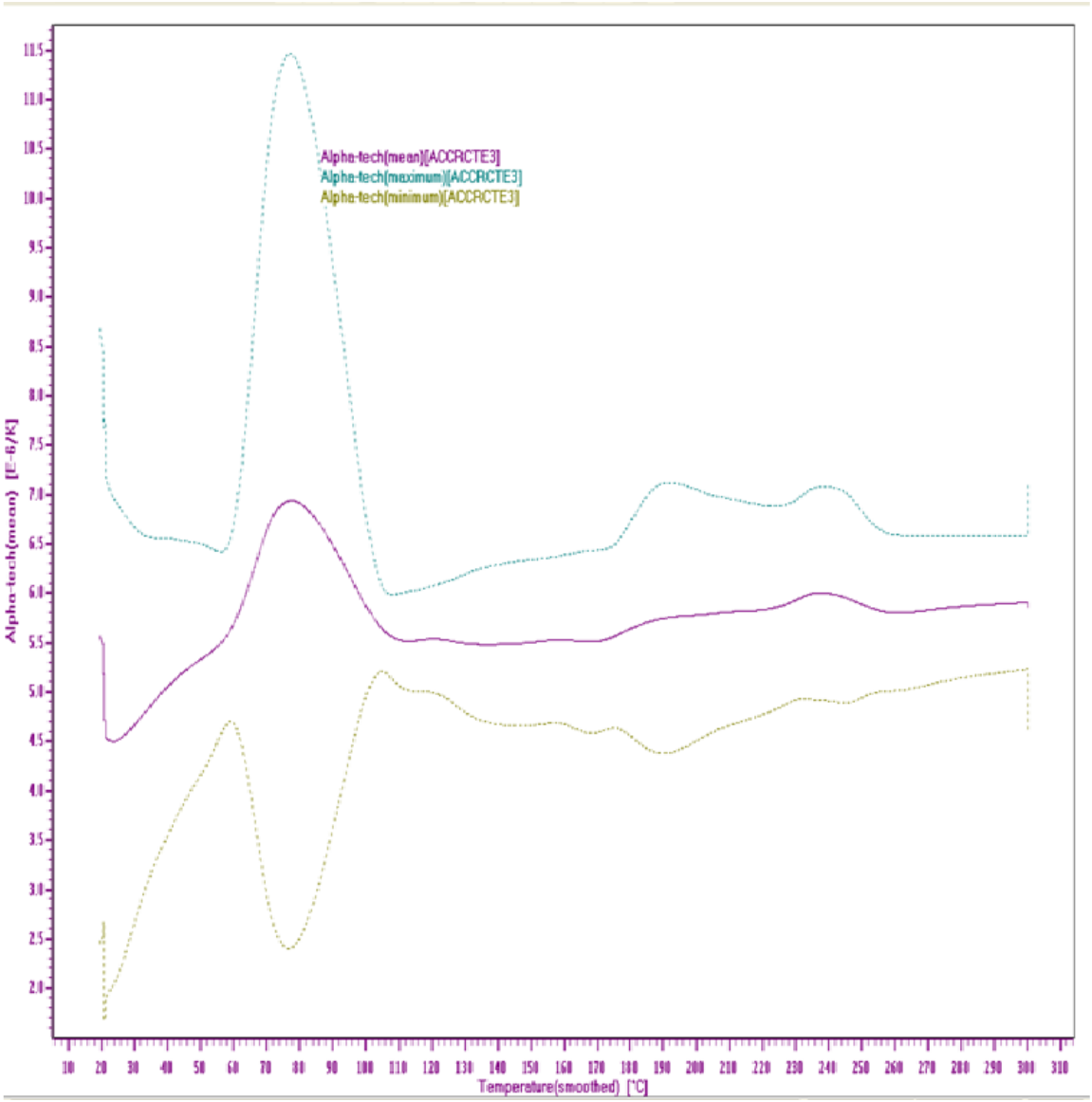

Fig 3.4 Maximum, minimum and mean of coefficient of thermal expansion curves for ACCR core samples

Fig 3.4 indicates that the coefficient of thermal expansion of the metal matrix core lies between $4.5\times10^{-6}/K$ and $6.5\times10^{-6}/K$ in the temperature range of 130℃ - 300℃. The mean, maximum and minimum of the coefficient of thermal expansion curves obtained from different tests on ACCC carbon fiber/epoxy core sample is given in Fig 3.5.

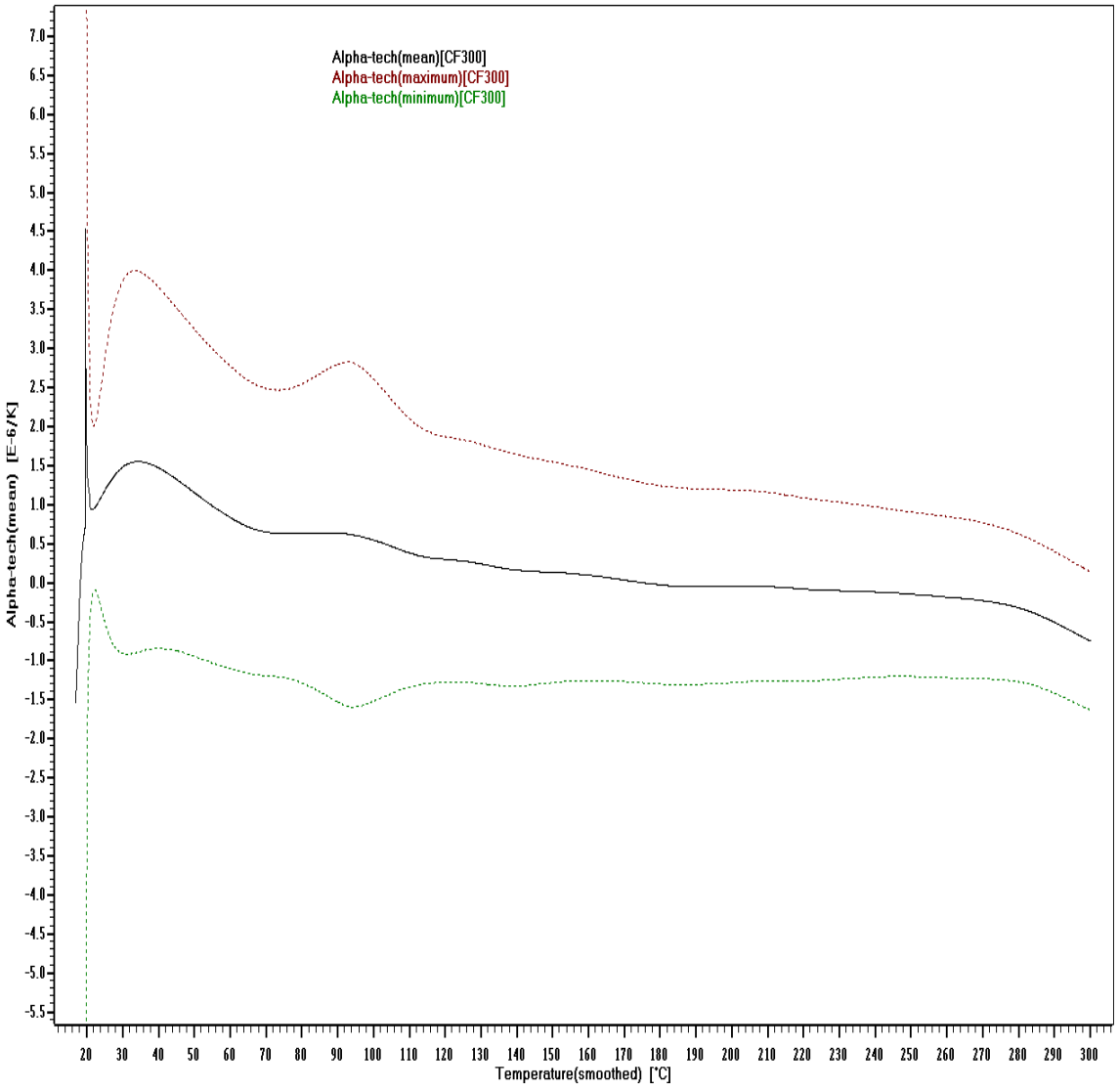

Fig 3.5 Maximum, minimum and mean of coefficient of thermal expansion curves for ACCC core samples

Fig 3.5 indicates that the coefficient of thermal expansion of the metal matrix core lies between $-1.0\times10^{-6}/K$ and $2\times10^{-6}/K$ for temperatures above 120°C. The average coefficient of thermal expansion α_{avg} of the ACCR core sample and the ACCC carbon finer/epoxy core sample in each test was calculated with the help of equation (3.2). The calculations are summarized in Tables 3.2 and 3.3.

Table 3.2
Summary of the average coefficient of thermal expansion (α_{avg}) calculations for the ACCR core sample

Test no	Change in length (μm)	Change in temperature (°C)	α_{avg} (10^{-6}/K)
1	16.52	280.5	5.837
2	16.72	279.2	5.923
3	17.78	279.8	6.293
4	15.81	283	5.534
5	16.4	282	5.756
6	17.58	279	6.243

The mean of the average coefficients of thermal expansion (α_{mean_avg}) of ACCR core sample calculated in each test were obtained with the help of the following equation (ambient - 300°C) –

$$\alpha_{mean\_avg(MMC)} = \frac{\alpha_{avg1} + \alpha_{avg2} + \alpha_{avg3} + \alpha_{avg4} + \alpha_{avg5} + \alpha_{avg6}}{6} \quad (3.3)$$

$$\alpha_{mean\_avg(MMC)} = 5.931\times10^{-6}/K \quad (3.4)$$

The standard deviation is,

$$S.D = \sqrt{\frac{\sum_{i=1}^{N}(\alpha_{avgi} - \alpha_{mean\_avg(MMC)})^2}{N}} \tag{3.5}$$

Where,

N = 6

$$S.D = 2.663 \times 10^{-7} / K \tag{3.6}$$

Thus, the average coefficient of thermal expansion of ACCR metal matrix core in the temperature range of ambient - 300℃ is $5.931 \times 10^{-6} / K$ according to the thermal mechanical analysis.

Table 3.3
Summary of the average coefficient of thermal expansion (α_{avg}) calculations for the ACCC CF/epoxy core sample

Test no	Change in length (μm)	Change in temperature (℃)	α_{avg} (10^{-6}/K)
1	-2.23	283	-0.799
2	-3.05	280.2	-1.102
3	-0.54	283	-0.193
4	-2.7	280.2	-0.974
5	-1.61	279.4	-0.584

The mean of the average coefficients of thermal expansion (α_{avg}) of ACCC carbon fiber/epoxy core sample calculated in each test (ambient - 300℃) –

$$\alpha_{mean\_avg(CF/epoxy)} = \frac{\alpha_{avg1} + \alpha_{avg2} + \alpha_{avg3} + \alpha_{avg4} + \alpha_{avg5}}{5} \tag{3.7}$$

$$\alpha_{mean\_avg(CF/epoxy)} = -0.731 \times 10^{-6} / K \tag{3.8}$$

The standard deviation is,

$$S.D = \sqrt{\frac{\sum_{i=1}^{N} (\alpha_{avgi} - \alpha_{mean\_avg(CF/epoxy)})^2}{N}} \tag{3.9}$$

Where,

N = 5

$$S.D = 3.202 \times 10^{-7} / K \tag{3.10}$$

Thus, the average coefficient of thermal expansion of ACCC carbon fiber/epoxy core in the temperature range of ambient - 300°C according to the thermal mechanical analysis is $-0.731 \times 10^{-6} / K$. The negative coefficient of thermal expansion of carbon fiber/epoxy and positive coefficient of glass fiber/epoxy in the ACCC composite core may cause significant thermal stress at the glass-carbon interface at elevated temperatures [34].

CHAPTER 4

DYNAMIC MECHANICAL ANALYSIS OF CARBON COMPOSITE CORES

Dynamic mechanical analysis (DMA) is a thermal analysis technique that is employed to determine the stiffness of a visco-elastic material [39], [40], [42]. It provides important information on the storage modulus, loss modulus and tan delta of the material. The carbon composite core of HTLS conductors is a visco-elastic material because of the presence of epoxy. It has been shown that the tensile strength of a unidirectional hybrid glass fiber-carbon fiber/epoxy matrix rod has a correlation to the storage modulus of the unidirectional carbon fiber/epoxy part of the rod [38]. This correlation indicates that the normalized values of storage modulus with temperature are equal to the normalized values of the tensile strength with temperature of the hybrid composite. Thus, DMA can be applied to the carbon composite cores of HTLS conductors to determine the variation of storage modulus with temperature. This will then give an estimate on the variation of the tensile strength of the HTLS carbon composite core. In this chapter, DMA of carbon fiber/epoxy matrix samples from ACCC core is described and the results and analysis is presented.

4.1 TA instruments DMA Q800

TA instruments DMA Q800 [54] was used for dynamic mechanical analysis of the carbon fiber/epoxy core of ACCC. The machine consists of a non-contact drive motor, which applies sinusoidal force for the sample deformation, a drive shaft for force guidance and optical encoder displacement sensor. A furnace provides temperature control with the help of two thermocouples. The thermocouples are located close to the clamps that hold the sample. The clamps have high stiffness and low mass. The clamp

consists of fixed and movable part. The moveable part is connected to the drive shaft. There are three different types of clamps depending on the mode of deformation. These modes of deformation are [54] –

1. Single/Dual cantilever bending mode – In this mode, the sample is clamped down at either ends or a single end by fixed clamps. A movable clamp applies the bending force at the center of the sample.
2. Tension mode – In this mode, the sample is placed in tension between a fixed and a moveable clamp. Thin films are particularly suited for this type of mode.
3. Compression mode – The sample is placed in compression between a fixed and a moveable plate.
4. Shear mode – Two pieces of the same sample is secured between two fixed plates and a moveable plate.
5. 3-Point bending mode – In this mode, the sample is supported at both ends and the moveable clamp applies the bending force.

Samples with rectangular geometry are suitable for single/dual cantilever or 3-point bending mode. The DMA Q800 can deliver a maximum force of 18 N and have a frequency range of 0.001 to 200 Hz. The temperature range in which it can operate is -150^{o}C to 600^{o}C. Special gas cooling accessory is required for sub ambient operation. DMA Q800 is capable of providing various modes of operation such as multi-frequency, multi-stress/strain, isostrain, creep/stress relaxation and controlled force/strain rate [54]. The system is connected to a computer that runs TA instruments DMA software. The DMA software has the capability to control, acquire and analyze the data from the experiments. Fig 4.1 shows the TA instrument DMA Q800 system.

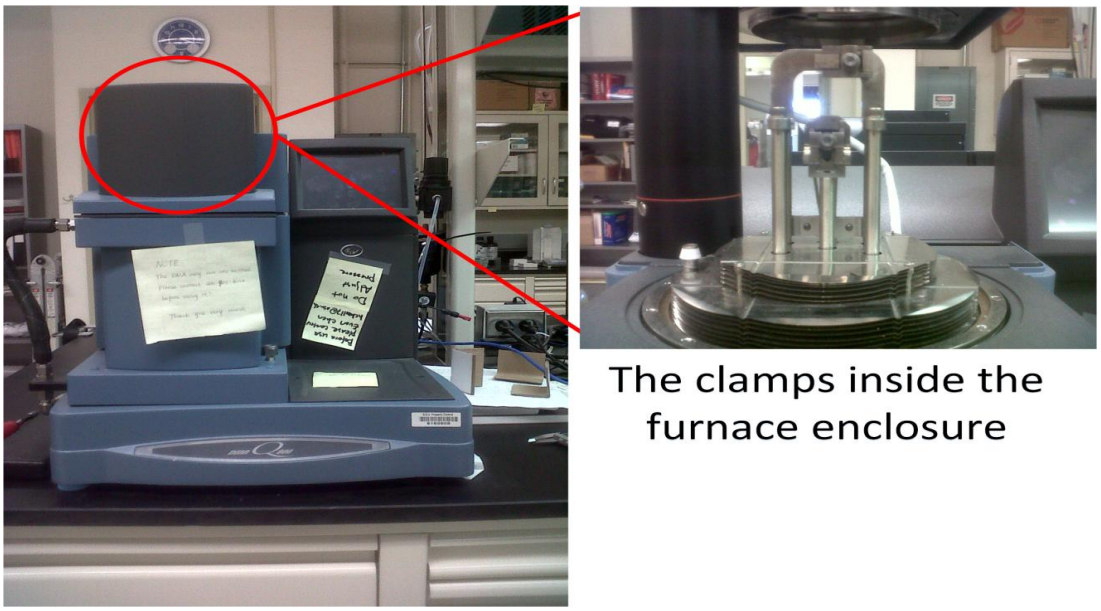

Fig 4.1 The dynamic mechanical analysis test system

4.2 Test details and procedure

DMA was performed on the samples with the help of TA instruments DMA Q800. The objective was to quantify the reduction in storage modulus with temperature and determine glass transition temperature of the samples. The mode of deformation chosen was the dual cantilever bending mode and dual cantilever clamps were installed. The samples were secured by the clamps with the help of a torque wrench set at 9 in-lbs. The mode of operation was multi-frequency mode at fixed frequency. An oscillating force of fixed frequency and amplitude 1 Hz and 20 µm respectively was applied perpendicular to the direction of the carbon fibers in the sample. A furnace covering the stage area holding the clamps achieved the heating of samples. The samples were heated from Ambient - 300^{o}C with a temperature ramp rate of 5^{o}C/min. The instrument and the clamps were calibrated in order to ensure accuracy of the data collected. The instrument and clamp calibration report is given in the Table 4.1 and 4.2 respectively. Several

samples, prior to the DMA experiments, were heat treated at 125°C, 175°C and 250°C for 120 hours in a muffle furnace. Data analysis was done with the help of TA instruments DMA software.

Table 4.1
DMA instrument calibration report

Type	Residual
Electronics	0.00007
Force	0.0029
Dynamic	0.0068
Position	Calibrated

Table 4.2
Clamp calibration report

Type	Mass	Offset	Compliance	Size
Dual Cantilever	29.5 gm	0.00 mm	0.181 µm/N	35 mm

1. DMA of untreated/ virgin samples - DMA with the conditions discussed above were performed on three untreated samples. The storage modulus and glass transition temperature of untreated samples were taken as the average of the three samples. One virgin sample was sent to Cambridge Polymer Group, Boston for DMA to determine the storage modulus variation with temperature of the sample. The result was received and is reproduced in appendix B.
2. DMA of heat treated samples – Twelve heat treated samples, with four samples in each heat treated batch (125°C, 175°C and 250°C), were subjected to DMA with

the above conditions. The storage modulus and the glass transition temperature values obtained for 125°C, 175°C and 250°C heat treated samples were averaged from the values of the four samples in each heat treated batch.

The data files gathered from the experiment were loaded into excel sheets and relevant graphs were plotted in MATLAB software. The data file includes information about storage modulus, loss modulus, temperature and tan delta values. Fig 4.2 shows the experimental setup.

Fig 4.2 DMA experimental setup

4.3 Sample description

Samples were machined out from the carbon fiber/epoxy composite part of DRAKE size ACCC core and had rectangular dimensions. It measured 60 mm in length, 4 mm in width and 1.6 mm in height. Samples were checked for any surface defects prior to the experiments. The samples consist of unidirectional carbon fibers embedded in

epoxy matrix. Fig 4.3 shows a carbon fiber fiber/epoxy composite sample from ACCC core.

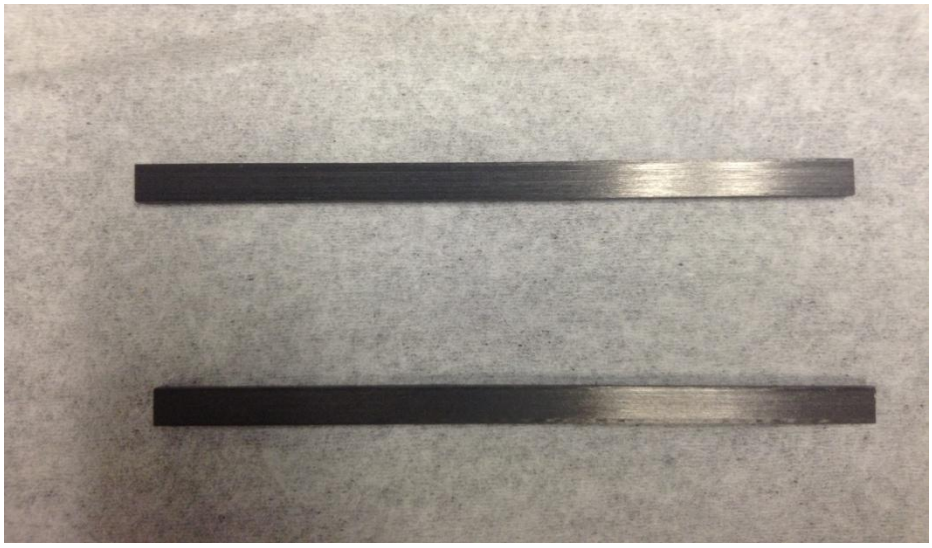

Fig 4.3 Carbon fiber/epoxy matrix samples from ACCC core

4.4 Results

Dynamic mechanical analysis provides the loss of storage modulus of ACCC carbon fiber/epoxy core with temperature. The loss in tensile strength of the ACCC carbon core from room temperature can be estimated from the storage modulus curve with temperature [38]. The error in the values between normalized storage modulus and normalized tensile strength of the conductor is normally less than 10% [38]. The peak of tan delta curve characterizes the glass transition temperature (T_g) of the sample. Fig 4.4 shows the loss in storage modulus and tan delta for the untreated samples. The graph shows the average values of storage modulus and tan delta of the three untreated samples. Similarly, the results of DMA on heat-treated samples are shown in Fig 4.5 – 4.7. Fig 4.8 compares the loss in storage modulus with temperature and the glass transition

temperature (characterized by the peak of the tan delta curve) of the untreated and heat-treated samples.

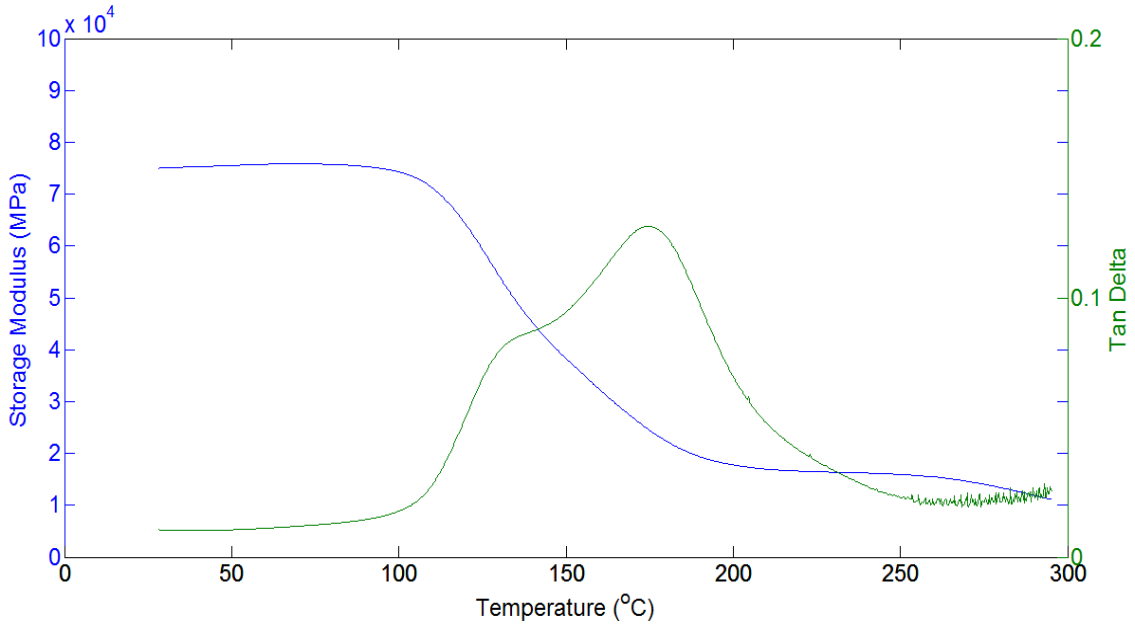

Fig 4.4 Storage modulus and tan delta of virgin samples

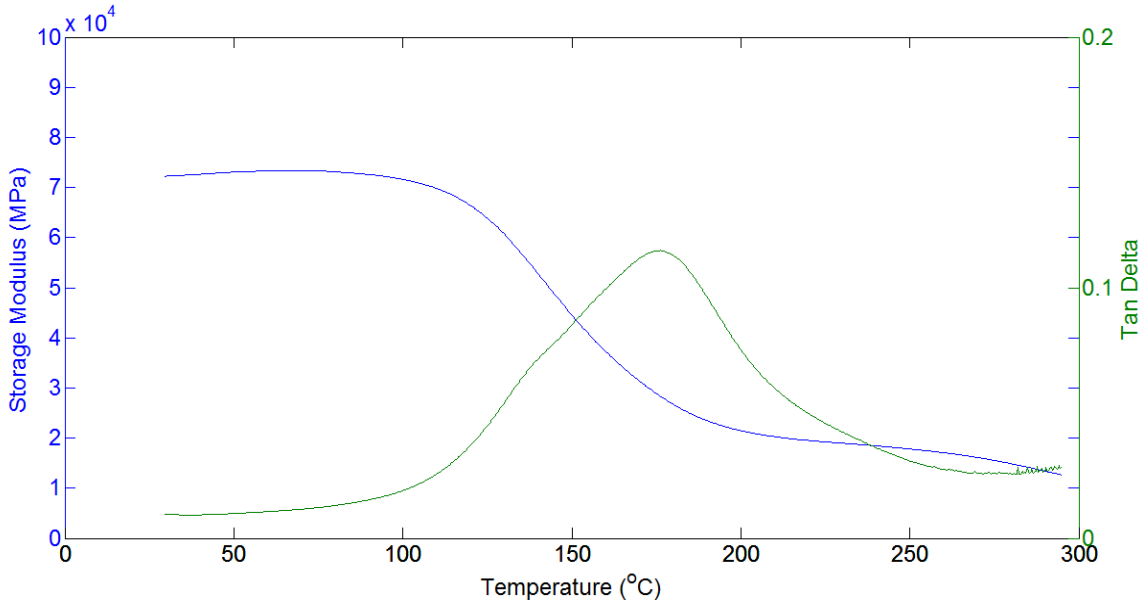

Fig 4.5 Storage modulus and tan delta of samples heat treated at 125°C

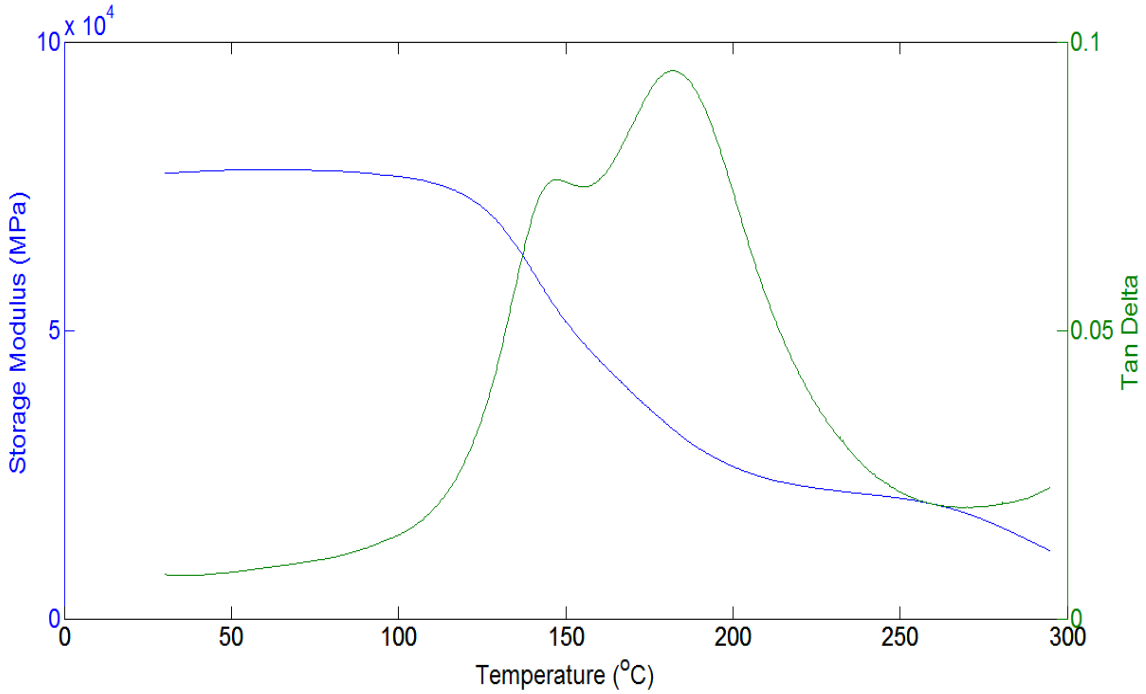

Fig 4.6 Storage modulus and tan delta of samples heat treated at 175°C

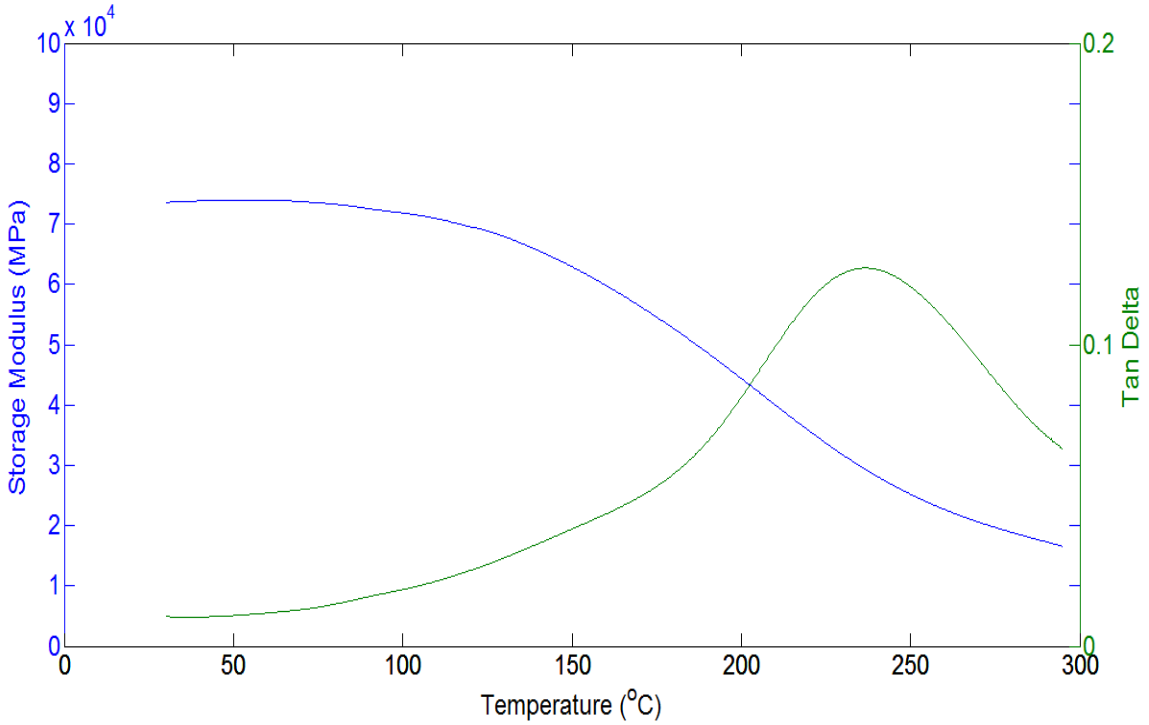

Fig 4.7 Storage modulus and tan delta of samples heat treated at 175°C

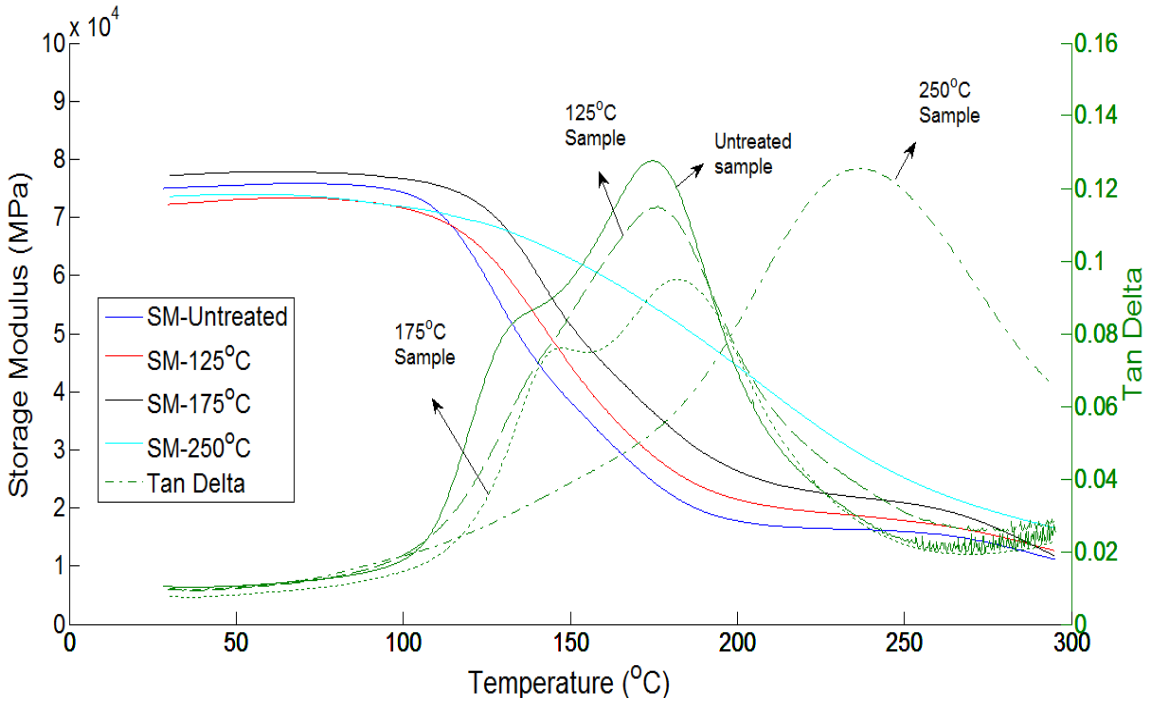

Fig 4.8 Comparison of DMA of untreated and heat – treated samples

DMA results of both untreated and heat treated samples, except 250°C heat-treated samples, indicate that the samples retain their storage modulus until 110°C - 120°C. This is followed by a rapid drop in storage modulus in the temperature range of 120°C - 200°C. The storage modulus plateaus after 200°C, which is followed by another drop in storage modulus after 250°C. For the 250°C heat-treated samples, the storage modulus is retained until 130°C. The decline of storage modulus for 250°C heat-treated samples is gentler compared to untreated and other heat treated samples. Fig 4.8 indicates that the slope of decline in storage modulus is the sharpest for the untreated samples and decreases progressively as the degree of heat-treatment of the samples increases. Fig 4.8 also show that the glass transition temperatures shift towards higher temperatures with increasing order of heat treatment of the samples. The observed shift in the glass

transition temperature can be explained by considering that the epoxy matrix of the untreated sample is not fully cured. Heat treatment of the samples increased the cross linked density of the matrix which raises the glass transition temperature. This is called post curing of epoxy [46], [55], [56]. Here, the heat treatment caused post curing of the epoxy matrix in the sample.

The glass transition temperature reflects the cure temperature if the cure temperature is less than the glass transition temperature of the fully cured network [56]. The cure plot of epoxy is available in reference [56]. However, if the cure temperature is greater than the glass transition temperature of the fully cured network of epoxy matrix, then the observed glass transition temperature would be less than the cure temperature [56]. Thus, three cases for the epoxy matrix, having a fully cured glass transition temperature of T_{Ginf}, cured or heat treated at T_o are described,

1. T_o less than T_{Ginf} – In this case, T_g becomes equal to T_o. As T_o increases, the T_g of the network correspondingly increases.
2. T_o equal to T_{Ginf} – In this case, T_g becomes equal to T_{Ginf}.
3. T_o is greater than T_{Ginf} – In this case, T_g is less than T_o. As T_o increases, the T_g of the network correspondingly decreases and vice versa. Degradation of the cross-link of the epoxy matrix takes place.

It is important to note here that the cross-linked network of epoxy eventually reaches full cure in a long time at ambient conditions [56]. Cure temperatures accelerate the process [55], [56]. The fact that the glass transition temperature increases after heat treatment of the samples shows that the epoxy matrix in the samples was not fully cured. From Fig 4.4, it can be seen the untreated samples had two tan delta peaks at around

132°C and 174°C. This indicates two polymerization reactions. For 125°C heat-treated samples, the glass transition temperature was 176°C approximately. This is almost equal to the glass transition temperature of the untreated samples. The glass transition temperature was 182°C for 175°C heat-treated samples. The glass transition temperature for 175°C heat-treated samples was greater than 175°C because of a small amount of additional post curing induced due to temperature scan until 300°C during DMA. However, for 250°C heat-treated samples, the glass transition temperature was 238°C, which is less than the post cure temperature (250°C). This shows that the heat treatment temperature of 250°C was more than the glass transition temperature of the fully cured network for epoxy matrix. Since the glass transition temperature of 250°C heat-treated samples was close to the temperature of heat treatment (250°C), the glass transition temperature of the fully cured network of the epoxy matrix of the samples was approximately 250°C.

4.5 Analysis

The results obtained from the DMA experiments were analyzed to quantify the loss of storage modulus (hence tensile strength of the ACCC composite core) with temperature. Table 4.3 summarizes the results for the DMA experiments and provides the loss of storage modulus (hence tensile strength) of the untreated and heat-treated samples at 125°C, 175°C and 250°C. The heat-treated samples retained their storage modulus (hence tensile strength) at ambient conditions after the heat treatment. The loss of storage modulus for untreated samples operating at 125°C, 175°C and 250°C were more than heat-treated samples. Heat treatment (post curing) of samples at or above 125°C

improved the storage modulus (hence tensile strength) characteristics, which can be attributed to increased cross-link density of the polymer due to post curing [55], [56].

Table 4.3
Summary of the DMA results

Temperature (°C)	Storage Modulus (°C)				Reduction in Storage Modulus (%)			
	Untreated Sample	Heat Treated Samples			Untreated Samples	Heat Treated Samples		
		125°C	175°C	250°C		125°C	175°C	250°C
Ambient	74977	72237	77209	73584	-	-	-	-
125°C	59163	63768	71375	68827	21	11	7	6
175°C	24356	28865	36318	54563	67	60	53	25
250°C	15935	17813	20873	25185	78	75	73	65

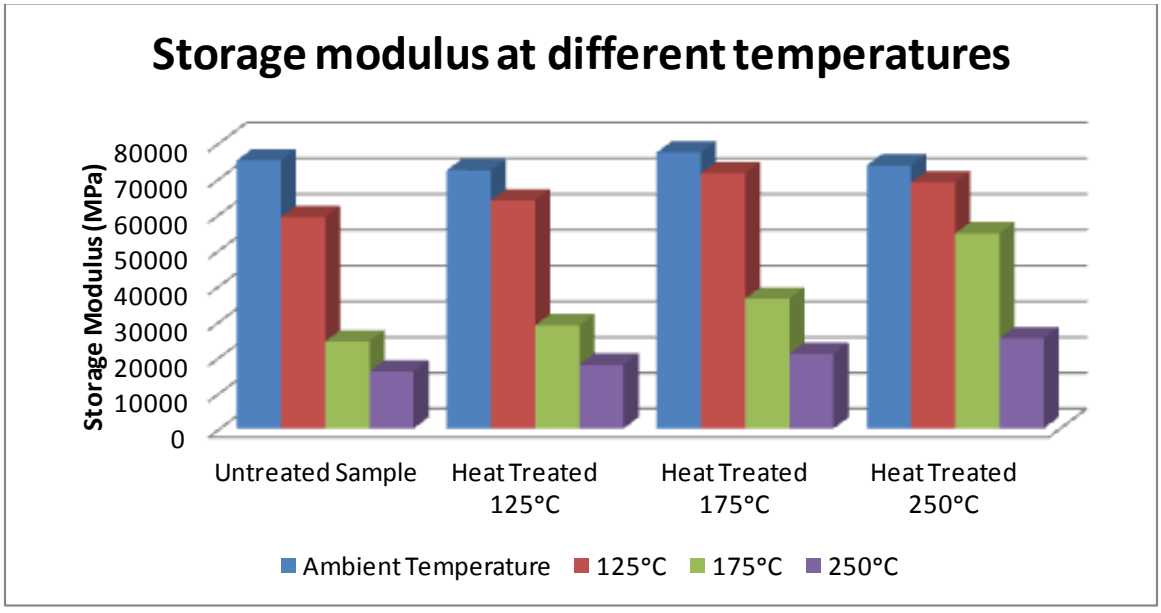

Fig 4.9 Graph showing storage modulus at different temperatures for the untreated and heat – treated samples

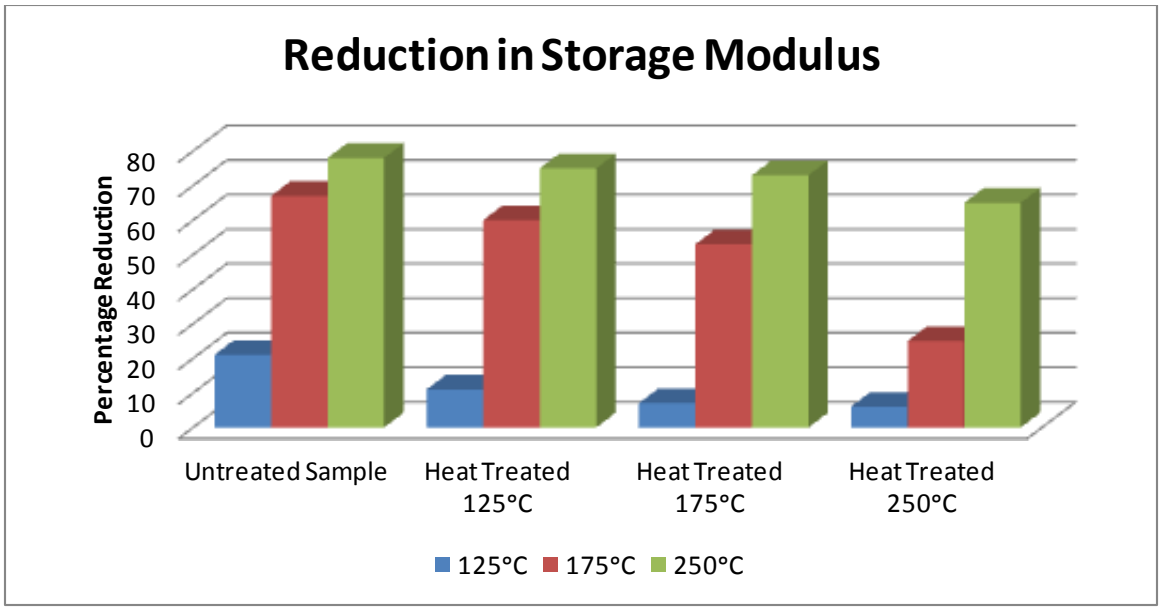

Fig 4.10 Graph showing reduction in storage modulus (hence tensile strength) at different temperatures for the samples

Equation (1.1) gives the relationship between the storage modulus of the carbon fiber/epoxy core and the tensile strength of the hybrid core of glass-carbon fiber/epoxy. The tensile strength of DRAKE size ACCC carbon core is 153.8 kN [11]. Thus, according to Table 4.3, the tensile strength of the DRAKE size ACCC carbon core will be around 81.5 kN, if the conductor is continuously operating at 175°C without any previous history of the conductor being subjected to temperatures above 175°C. This is a reduction around 50%. Lastly, the results indicate that the glass transition temperature of fully cured epoxy matrix (T_{Ginf}) lies around 250°C. If the conductor is subjected to temperatures above T_{Ginf} for a long period (>120 hrs), then permanent degradation of fiber-epoxy interface may occur reducing the tensile strength of the conductor permanently.

CHAPTER 5

TENSILE TESTING OF METAL MATRIX CORES

This chapter describes the tensile testing of ACCR metal matrix core. In order to understand the loss of tensile strength of ACCR core with temperature in laboratory, it is important to first test the loading of the core with appropriate gripping fixtures successfully. Custom grips were developed for the tensile testing of the ACCR core strand. Stress strain curve was also calculated from the load displacement curve of the metal matrix core specimen.

5.1 Development of custom gripping fixtures

A custom-made gripping fixture was developed for the tensile testing of the metal matrix core. The new grips work on the principle of friction force. It consists of three parts. The 3-D model of the custom grip is shown in Fig 5.1.

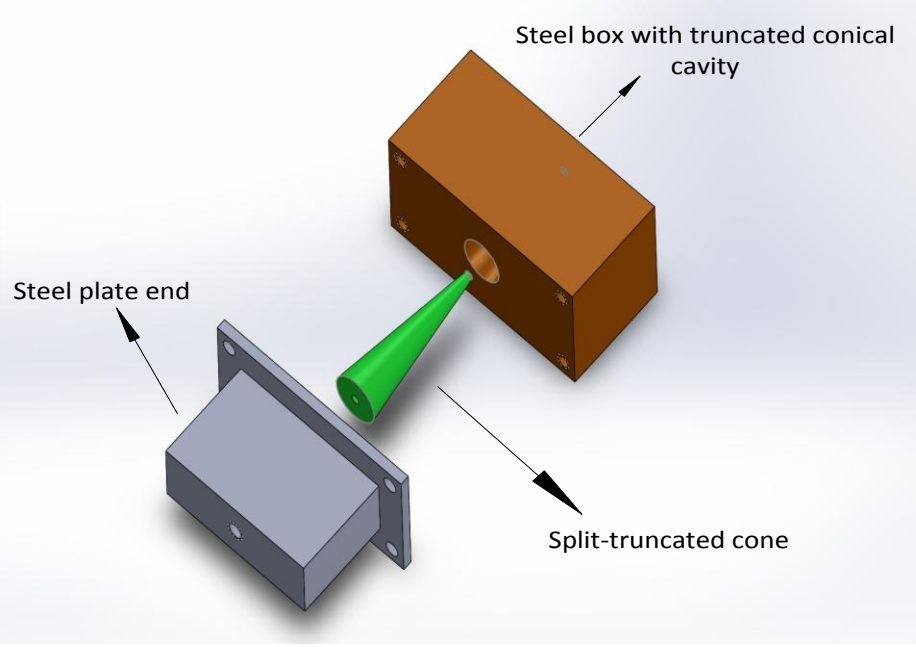

Fig 5.1 3-D model of the custom grip

The first part is made up of a steel box of dimensions 80 mm x 40 mm x 40 mm with a truncated cone cavity in the middle of the steel box. The diameter of the smaller circle of the truncated cone cavity is 3 mm and is at the top face of the steel box. The angle of the cavity is approximately 10 degrees. Four to eight female portion of screw connectors of size/thread 10-32 were drilled at the bottom of the steel box. The second part consists of truncated cone split into two halves along its diameter. The smaller mouth has an inner diameter of 2.8 mm and the outer diameter of 3 mm. The angle of the truncated cone is 10 degrees. The interior portion of the two halves of truncated cone have semi cylindrical cavity of diameter 2.8 mm. This is shown in Fig 5.2.

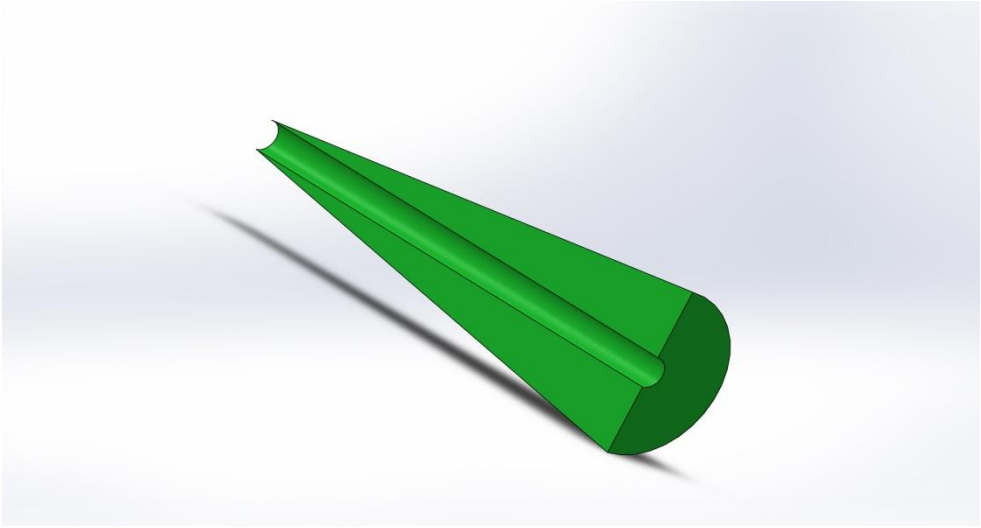

Fig 5.2 3-D model of split truncated cone

The split-truncated cone wraps around and holds one end of the specimen. The third part consists of a steel plate of dimension 8cm x 4 cm x 0.35 cm with rectangular steel back of dimensions 60 m x 40 mm x 36.5 mm. The steel back contains the female portion of screw connector of size/thread ¼ - 20 that helps in connecting the gripping fixture to the load frame. The steel plate has eight clearance holes for screw size/thread

10-32. The two halves of the truncated cone with one end of the specimen fit together in the cavity of the steel box with a portion of the split-truncated cone protruding about 5 mm out from the bottom of the steel box. It is secured in the place by the steel plate pushing from the bottom with the help of four or eight screw size/thread 10-32. The force exerted by the steel plate on the split-truncated cone allows tight gripping of the specimen by compressing the top ends of the split truncated cones. The friction force between the specimen and the interior of the truncated cone holds the specimen in place.

5.2 Sample description

Specimens were alumina fiber/aluminum matrix composite rods obtained from the metal matrix core of ACCR composite conductor. The specimen rod was 2.3 mm in diameter and 127 mm long. The ultimate tensile strength of these metal matrix composite rods is approximately 1400 MPa [44]. Fig 5.3 shows the sample with the custom grips.

Fig 5.3 ACCR core strand sample held by the custom grips

5.3 Experimental Setup

Tensile test on the metal matrix core strand was performed at room temperature using the INSTRON 4411 MTS test system [57]. The system consists of a load frame and a control console. The load frame provides tension or compression force to the specimen mounted on it. Control console performs calibration and controls the test with the help of feedback control systems. The test setup conditions are inputted through the front panel attached to the load frame. The load frame have cross-head drive motor, which applies tension or compression by moving the crosshead upwards or downwards. A load transducer measures the applied load on the specimen. A general purpose instrument bus (GBIP) provides for data connection with a personal computer. The GBIP conforms to the IEEE 488 interface standard. The schematic diagram of the experimental setup is shown in Fig 5.4.

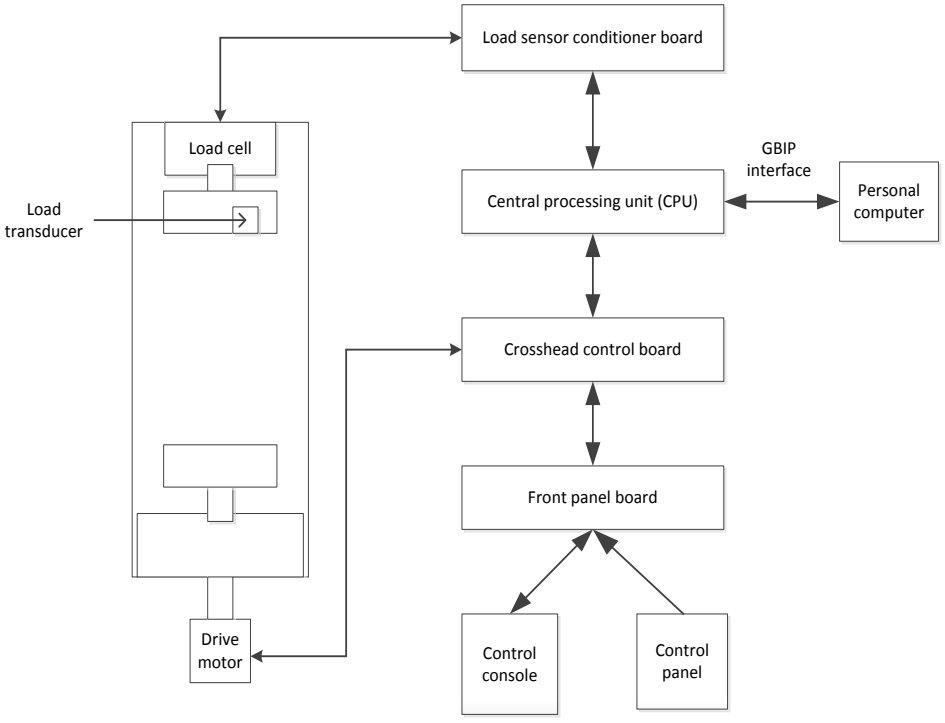

Fig 5.4 Schematic diagram of the INSTRON 4411 test system

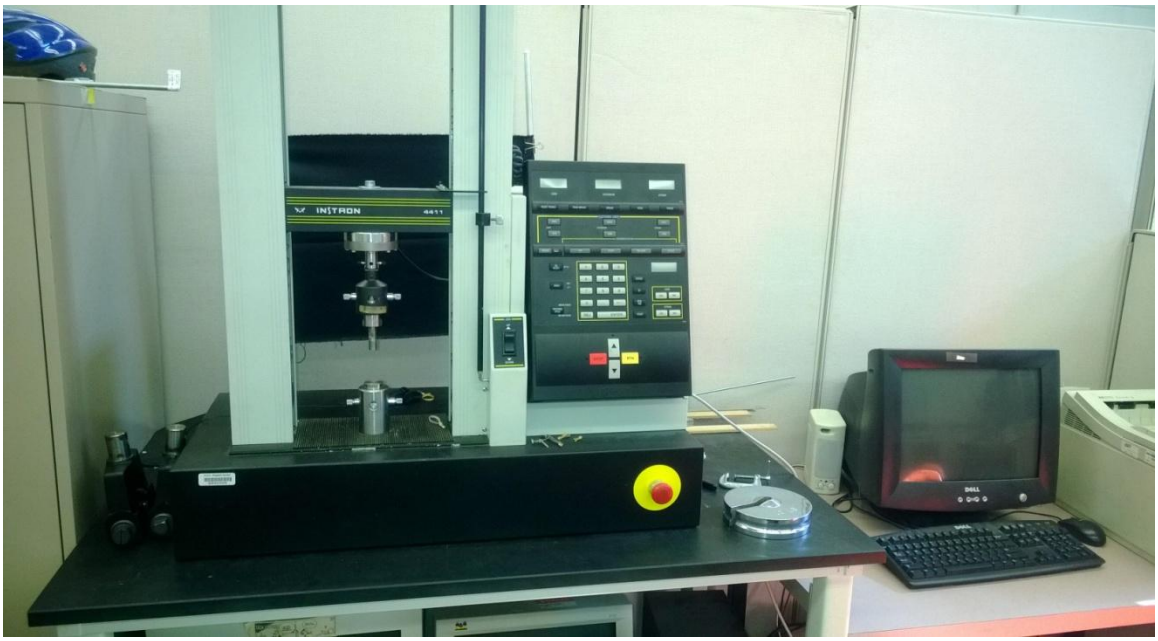

Fig 5.5 The INSTRON 4411 MTS system interfaced to a personal computer

5.4 Test details and procedure

Tensile test of ACCR metal matrix core was performed using INSTRON testing machine with 5 kN load cell at room temperature. The specimen was loaded in the custom gripping fixture that was then secured to the load frame and is shown in Fig 5.6. The gauge length of the specimen was 1.89 inches. The crosshead speed was set at 2 mm/min and a data rate of 5 pts/sec was enabled by the machine's data acquisition system. The test was carried out until the machine reached its maximum load limit of 5 kN. The load – displacement results was used to calculate the stress-strain curves of the specimens. The initial test was conducted with the grips having only four screws on each fixture. This lead to reduced friction between the sample and the grips since the force on the truncated cones by the steel plate was not enough. The result was slippage of the sample inside the gripping fixtures.

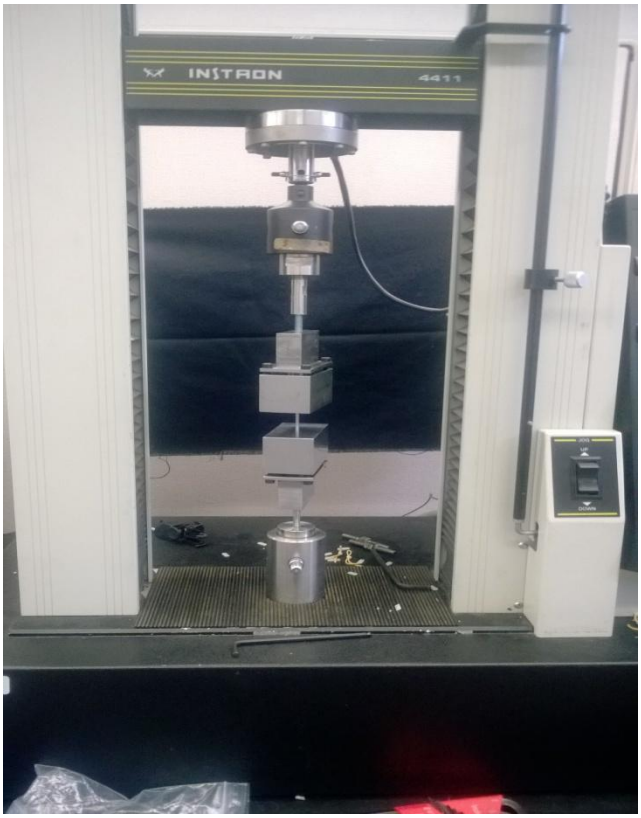

Fig 5.6 Specimen mounted on the load frame with the custom grips

Fig 5.7 Specimen loaded at 5 kN with the help of the custom gripping fixtures on the test frame

The custom grips were fitted with four more screws in order to increase the force on the truncated cone by the steel plate. This increased the friction force between the specimen and the interior of the truncated cone. In the subsequent test, the specimen was successfully loaded to 5 kN. Fig 5.7 shows the metal matrix core specimen successfully loaded to 5kN.

5.5 Results

Load displacement graphs were obtained from the tensile tests. The load displacement plots are given in Fig 5.8 and 5.9. In the first test, slippage of the specimen occurred inside the gripping fixture. This problem was addressed by introducing another four new screw connectors between the steel box and the plate in order to increase the force on the truncated cone. Thus, the total number of screw connectors for the grips in the second test was eight. This resulted in increase of friction force on the specimen. The tensile test data for the two tests are given below in Table 5.1.

Table 5.1
Tensile test data for ACCR core strand specimen

Parameter	Test 1	Test 2
Maximum load, kN	3.48	5
Maximum displacement, mm	26.03	2.13
Modulus of elasticity, GPa	-	62.34

5.6 Analysis

The test data were analyzed to produce the stress-strain plot for the test 2, in which the specimen was successfully loaded to 5 kN. The stress strain plot for test 2 is given in the Fig 5.10.

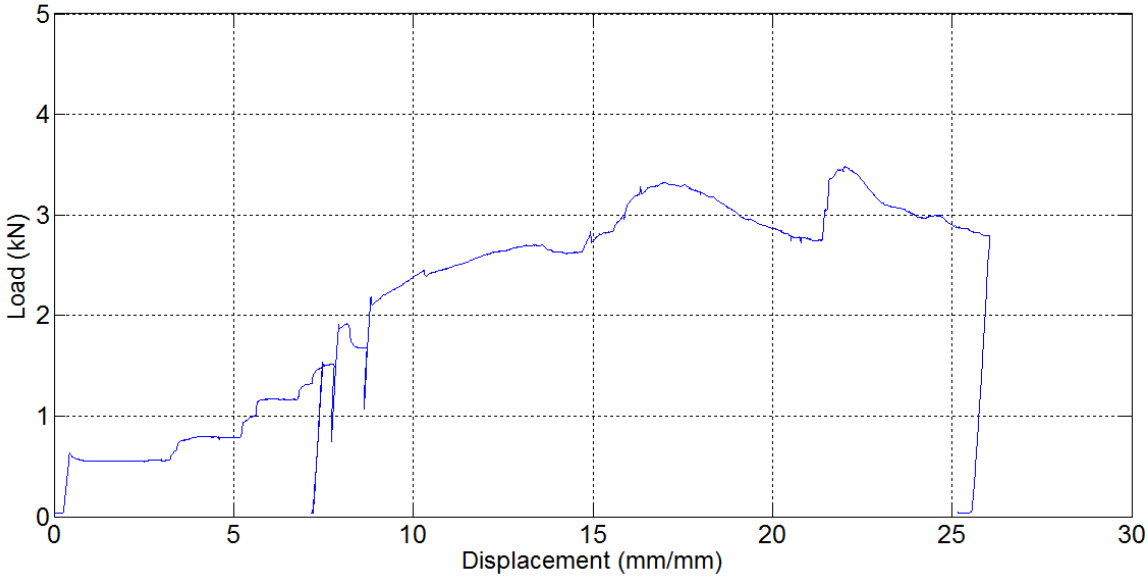

Fig 5.8 Load –Displacement plot for test 1

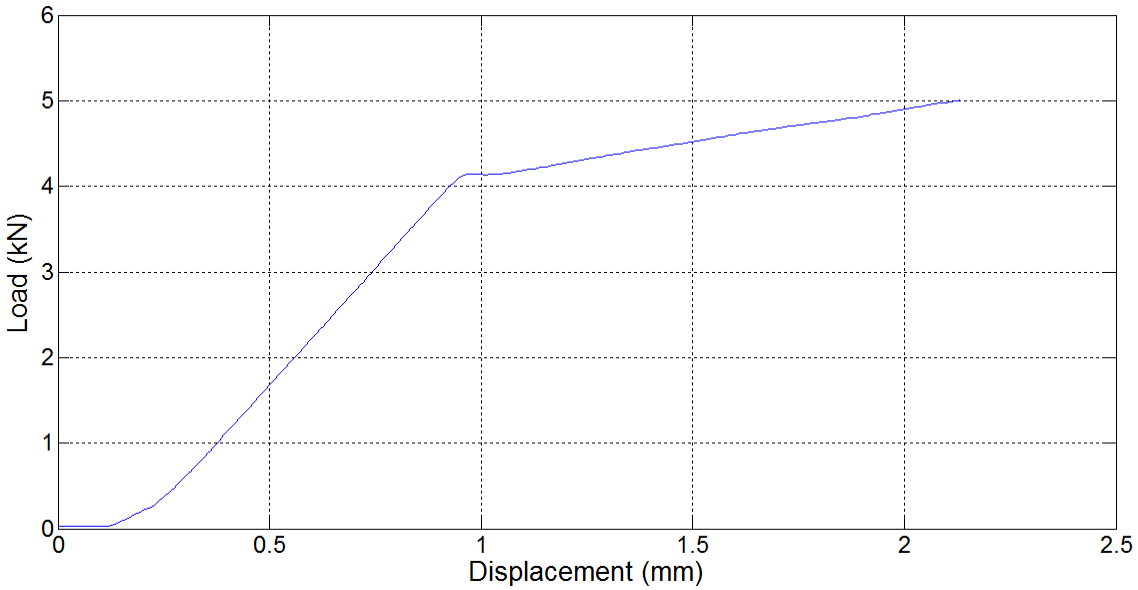

Fig 5.9 Load-Displacement plot for test 2

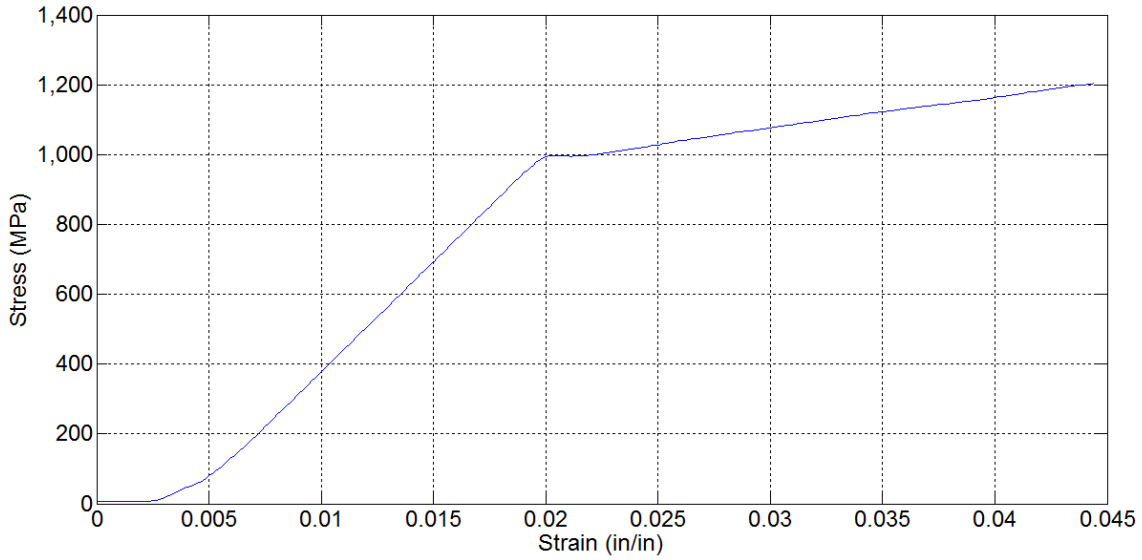

Fig 5.10 Stress-Strain plot for ACCR metal matrix core strand specimen in test 2

It is important to note that the stress vector is obtained by dividing the load vector with the cross sectional area of the specimen and the strain vector is obtained by dividing the displacement vector with the gauge length of the specimen. In literature, the reported value of tensile strength of ACCR metal matrix core strand at room temperature is approximately 1400 MPa [44]. The specimen was successfully loaded up to 1200 MPa. This corresponded to the maximum machine capability of 5 kN. Thus, further loading of the specimen was not possible. The elastic modulus of the ACCR metal matrix core strand was calculated as 62.34 GPa

It can be seen from the stress strain plot that the slope changes at a strain of 0.02 mm/mm and corresponding to a stress of 1000 MPa. This change of slope can be due to the physical changes in aluminum matrix, which is a ductile material. Ductile material exhibits a yield point as opposed to brittle material [58]. The alumina fibers in the conductor are brittle material and the aluminum matrix is ductile. The change of slope may thus represent the yield point of the specimen. At the yield point, microplasticity

occurs in the matrix that can be characterized by stress concentration in the matrix near sharp ends of the fiber [59]. However, the change of slope can also be explained by a small amount of slippage of the specimen in the gripping fixtures. Slippage of the specimen can be remedied with the help of an abrasive material such as silicon carbide gel between the specimen and the interior of the truncated cone. This will increase the friction force and may prevent slippage.

CHAPTER 6

THERMAL RATINGS AND CURRENT TEMPERATURE RELATIONSHIP OF HTLS CONDUCTORS

Current flowing through a conductor causes its temperature to rise. Temperature rise after a certain limit can cause thermal degradation of the conductor and may compromise its operation. Temperature rise affects the resistance, mechanical strength and thermal expansion of the conductor [20], [21]. Increased sag is a direct consequence of the temperature rise of the conductor due to increased power flow in the line. High temperatures can cause a conductor to sag below its sagging limit. The annealing of the conductor due to high temperatures causes loss of tensile strength [18]. In case of carbon composite core of HTLS conductors, high temperatures can cause degradation of the core, which may lead to loss of tensile strength of the conductor. Thus, the continuous current that a conductor can carry should be calculated so that the operating temperature it produces should not cause significant annealing or loss in tensile strength and sagging limits are not violated. Conservative ambient weather conditions is used in order to calculate the steady state thermal rating which allows for increased power flow during emergency conditions [21]. The conductor temperature depends on various other parameters, apart from heat loss due to current flow, such as convection heat loss, radiation heat loss and solar heat gain. Ambient weather parameters and conductor electrical resistance also play an important role in determining the conductor operating temperature. The conductor heat capacity contributes to the rate of rise of conductor temperature during transient conditions. In this chapter, IEEE 738-2006 [21] has been

utilized to calculate the steady-state thermal rating and current temperature relationship of HTLS conductors. Transient operation of HTLS conductors has been studied with the help of IEEE 738 standard and fault current temperature relationships have been developed for ACCC and ACCR.

6.1 Steady-state thermal calculations

The steady state heat balance operation results in a steady operating temperature for the conductor at a given operating current assuming that the ambient weather parameters remain constant. The steady state heat balance operation depends on various heat loss and gain rates [21]. This has been described in the subsequent subsections.

6.1.1 Steady-state heat balance

The steady state heat balance equation shows that the sum of heat loss due to current flow and solar heat gain of the conductor balances the conductor heat loss due to convection and radiation. The convection heat loss depends on forced convection and natural convection. The steady-state heat balance equation for a conductor carrying a current I (A) and having a resistance R (Ω/m) at temperature T_c (°C) is given below,

$$q_c + q_r = q_s + I^2 R(T_c) \tag{6.1}$$

Where,

q_c is the convection heat loss in W/m,

q_r is the radiation heat loss in W/m,

q_s is the solar heat gain in W/m,

$I^2 R(T_c)$ is the ohmic heat gain in W/m.

From equation (6.1), the current in the conductor is,

$$I = \sqrt{\frac{q_c + q_r - q_s}{R(T_c)}} \tag{6.2}$$

6.1.2 Forced convection heat loss

Convective heat loss is one of the major sources of heat loss from the conductor. Forced convection heat loss occurs when wind flow is present on the conductor. There are two equations which address the convection heat loss produced due to high and low wind speeds. For low wind speed the equation for the forced convection heat loss rate is,

$$q_{c1} = \left[1.01 + 0.0372\left(\frac{D\rho_f V_w}{\mu_f}\right)^{0.52}\right] k_f K_{angle}(T_c - T_a) \tag{6.3}$$

The equation for high wind speed is,

$$q_{c2} = \left[0.0119\left(\frac{D\rho_f V_w}{\mu_f}\right)^{0.6}\right] k_f K_{angle}(T_c - T_a) \tag{6.4}$$

Where,

q_c is convection heat loss rate in W/m,

D is the conductor diameter in mm,

ρ_f is the air density in kg/m^3 at temperature T_f,

V_w is the wind speed in m/s,

μ_f is the dynamic viscosity of air in Pa-s at temperature T_f,

k_f is the thermal conductivity of air in W/(m-°C) at temperature T_f,

K_{angle} is the wind direction factor,

T_c is the conductor temperature in °C,

T_a is the ambient temperature in °C.

The temperature T_f, in degrees, is given by,

$$T_f = \frac{T_c + T_a}{2} \tag{6.5}$$

This is the temperature of the thin film around the conductor. The wind direction factor is given by,

$$K_{angle} = 1.194 - \cos(\phi) + 0.194\cos(2\phi) + 0.368\sin(2\phi) \tag{6.6}$$

Where,

ϕ is the angle between the wind direction and the conductor axis, in degrees.

The wind direction factor can also be expressed in terms of the compliment of the angle between wind direction and the conductor axis.

$$K_{angle} = 1.194 - \sin(\beta) - 0.194\cos(2\beta) + 0.368\sin(2\beta) \tag{6.7}$$

Where,

β is the angle between the wind direction and perpendicular to the conductor axis, in degrees.

6.1.3 Natural convection heat loss

The natural convection heat loss is shown below,

$$q_{cn} = 0.0205\rho_f^{0.5} D^{0.75}\left(T_c - T_a\right)^{1.25} \tag{6.8}$$

Where,

D is the conductor diameter in mm,

ρ_f is the air density in kg/m^3 at temperature T_f,

T_c is the conductor temperature in °C,

T_a is the ambient temperature in °C.

Natural convection occurs when there is no wind flowing around the conductor. The IEEE current-temperature standard [21] recommends using the higher value of convection heat loss obtained from forced convection heat loss equation and natural convection heat loss equation for conservative calculations. Vector sum of forced convection and natural convection values can be used but it is not conservative.

6.1.4 Solar heat gain

The solar heat gain imparts heat to the conductor and consequently raises its temperature. The solar heat gain rate depends on the angle of incidence of the sun, the projected area of the conductor, the absorptivity and the total heat flux received by the conductor. For conservative calculations, the angle of incidence is taken as 90 degrees. The solar heat gain is,

$$q_s = \alpha_{ab} Q_{se} \sin(\theta) A' \tag{6.9}$$

Where,

α_{ab} is solar absorptivity,

Q_{se} is total heat flux received in W/m^2,

θ is the angle of incidence in degrees,

A' is the projected area of the conductor per unit length.

The angle of incidence is calculated with the help of the following equation,

$$\theta = \arccos[\cos(H_c)\cos(Z_c - Z_L)] \tag{6.10}$$

Where,

H_c is the altitude of the sun in degrees,

Z_c is the azimuth of the sun in degrees,

Z_L is the azimuth of the transmission line in degrees.

The azimuth of the transmission line is 90° or 270° for a line running in the east – west direction, whereas it is 0° or 180° for a line running in the north south direction [21].

6.1.5 Radiation heat loss

The conductor also loses heat through radiation, although to a lesser extent as compared to convection heat loss. The radiation heat loss is,

$$q_r = 0.0178 D \varepsilon \left[\left(\frac{T_c + 273}{100} \right)^4 - \left(\frac{T_a + 273}{100} \right)^4 \right] \tag{6.11}$$

Where,

D is the conductor diameter in mm,

ε is the emissivity,

T_c is the conductor temperature in °C,

T_a is the ambient temperature in °C.

6.1.6 Conductor resistance

For calculation of thermal ratings of the conductor, a linear function of the electrical resistance with temperature is considered. This is given in equation (6.12),

$$R(T_c) = \left[\left(\frac{R(T_H) - R(T_L)}{T_H - T_L} \right) \right] (T_c - T_L) + R(T_L) \tag{6.12}$$

Where,

$R(T_c)$ is the resistance of the conductor at temperature T_c, in Ω,

$R(T_H)$ is the resistance of the conductor at temperature T_H, in Ω,

$R(T_L)$ is the resistance of the conductor at temperature T_L, in Ω,

T_c is the conductor temperature in which new resistance is being calculated, in °C,

T_H is the conductor temperature in which resistance $R(T_H)$ is given, in °C,

T_L is the conductor temperature in which resistance $R(T_L)$ is given, in °C,

The function calculates AC electrical resistance. It is known that the electrical resistivity of common metals like aluminum increases in a non-linear fashion with temperature [21]. If the conductor temperature at which the resistance is desired lies between T_H and T_L, then the calculated resistance will higher than the actual resistance and thus will result in a conservative calculation. However, in most cases the error will be negligible. If conductor temperature, at which the resistance is desired, is higher than T_H, then the calculated resistance value would be lower than the actual resistance at that temperature. According to IEEE 738 standard [21], the resistance value for 1350 H19 aluminum strand at 500°C calculated from equation (6.12) is 5% lower than the actual value, when the resistance of the aluminum strand is given at 25°C (T_L) and 75°C (T_H).

6.1.7 Steady state ampacity rating for HTLS conductors

In this section, steady state thermal/ampacity ratings for HTLS conductors have been calculated with the help of a C++ program developed in Microsoft Visual Studio. The program employed the IEEE 738-2006 standard [21] for calculating the thermal steady state ratings. Table 6.1 outlines the input conditions for the program. The results for steady state ampacity rating of ACCR and ACCC for the conditions described in Table 6.1 is given in Table 6.2

Table 6.1
Input parameters for thermal steady state rating

Input Parameters	ACCR	ACCC
Wind speed (m/s)	0.61	0.61
Conductor elevation (m)	0	0
Emissivity	0.5	0.5
Solar absorptivity	0.5	0.5
Ambient temperature (°C)	40	40
Maximum temperature (°C)	210/240	180/200
Latitude (°)	43	43
Conductor diameter (mm)	28.12	28.12
Angle between conductor axis and wind direction (°)	90	90
Day number	161	161
Solar hour	14	14
AC resistance at 25°C (Ω/mile)	0.112	0.089
AC resistance at 75°C (Ω/mile)	0.134	0.106

Table 6.2
Steady state ampacity rating of ACCR and ACCC conductors

Conductor type (DRAKE)	Steady state ampacity rating	
	Continuous operation	Emergency operation
ACCR	1645 A	1770 A
ACCC	1700 A	1820 A

The continuous operating temperature of ACCR is 210°C and of ACCC is 180°C. The emergency temperature of ACCR is 240°C and of ACCC is 200°C. It can be seen from Table 6.2 that the ampacity of ACCC is greater than ACCR at both continuous operating temperature and emergency temperature, even though the continuous operating and emergency temperatures of ACCC is lower than ACCR.

6.1.8 Current – temperature relationship of HTLS conductors

A C++ program was developed to compute the current-temperature relationship of ACCC and ACCR conductors. The program also calculated ACSR conductor current temperature relationship, which was plotted with the HTLS conductors for comparison. The approach prescribed in IEEE 738 standard [21] was followed in the program. Data of current temperature relationship of ACSR, ACCC and ACCR obtained from C++ program are plotted between percent current on x-axis and temperature on y-axis. The base current in the plots is the current rating of equivalent ACSR at 100°C. Different conductor sizes have been considered namely DRAKE, LAPWING and BLUEBIRD. The assumptions for the calculation of data are following.

1. Clear atmosphere is assumed.
2. Angle of incidence of the sun is taken as 90 degrees for conservative calculations.

The general input parameters are given in Table 6.3. Specific input parameters for DRAKE, LAPWING and BLUEBIRD size conductors are given in Table 6.4 -6.6. The current temperature relationships for these conductors are given in Fig 6.1-6.3.

Table 6.3
Input parameters for current-temperature relationship

Input Parameters	Value
Wind speed (m/s)	0.61
Conductor elevation (m)	0
Emissivity	0.5
Solar absorptivity	0.5
Ambient temperature (°C)	40
Latitude (°)	43
Angle between conductor axis and wind direction (°)	90
Day number	161
Solar hour	14

Table 6.4
Conductor specific (DRAKE) input parameters for current temperature relationship

Input parameters	ACSR	ACCR	ACCC
Conductor diameter (mm)	28.1	28.1	28.1
AC resistance at 25°C (Ω/mile)	0.117	0.112	0.089
AC resistance at 75°C (Ω/mile)	0.139	0.134	0.106

Table 6.5
Conductor specific (LAPWING) input parameters for current temperature relationship

Input parameters	ACSR	ACCR	ACCC
Conductor diameter (mm)	38.2	38.9	38.2
AC resistance at 25°C (Ω/mile)	0.0617	0.0576	0.0507
AC resistance at 75°C (Ω/mile)	0.0728	0.069	0.0595

Table 6.6
Conductor specific (BLUEBIRD) input parameters for current temperature relationship

Input Parameter	ACSR	ACCC
Conductor diameter (mm)	44.75	44.75
AC resistance at 25°C (Ω/mile)	0.0475	0.0387
AC resistance at 75°C (Ω/mile)	0.0554	0.0447

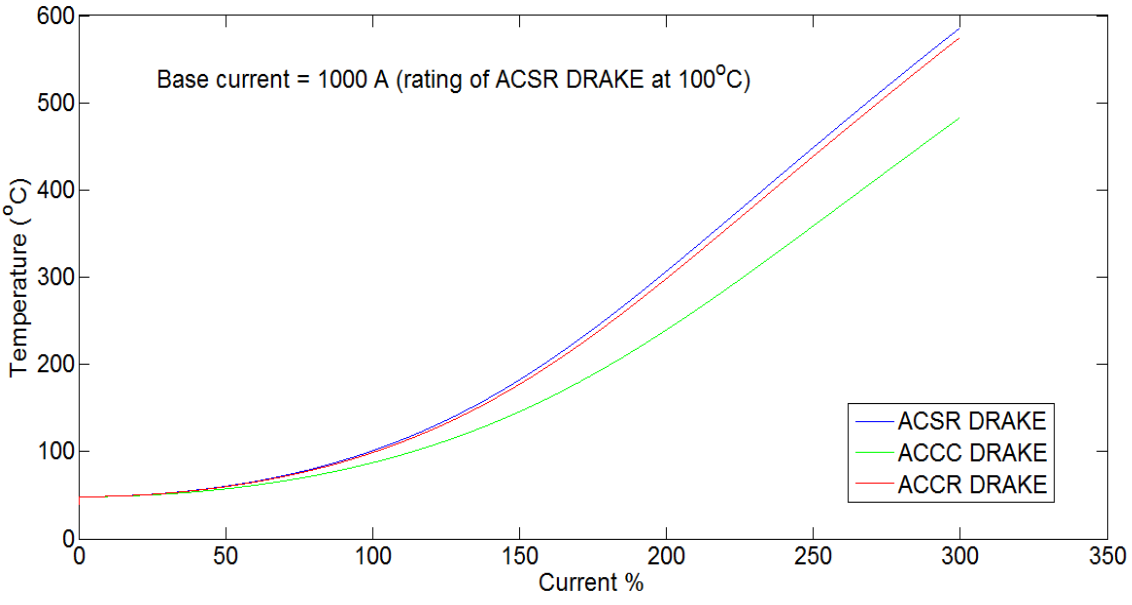

Fig 6.1 Current-temperature relationship of DRAKE sized conductors

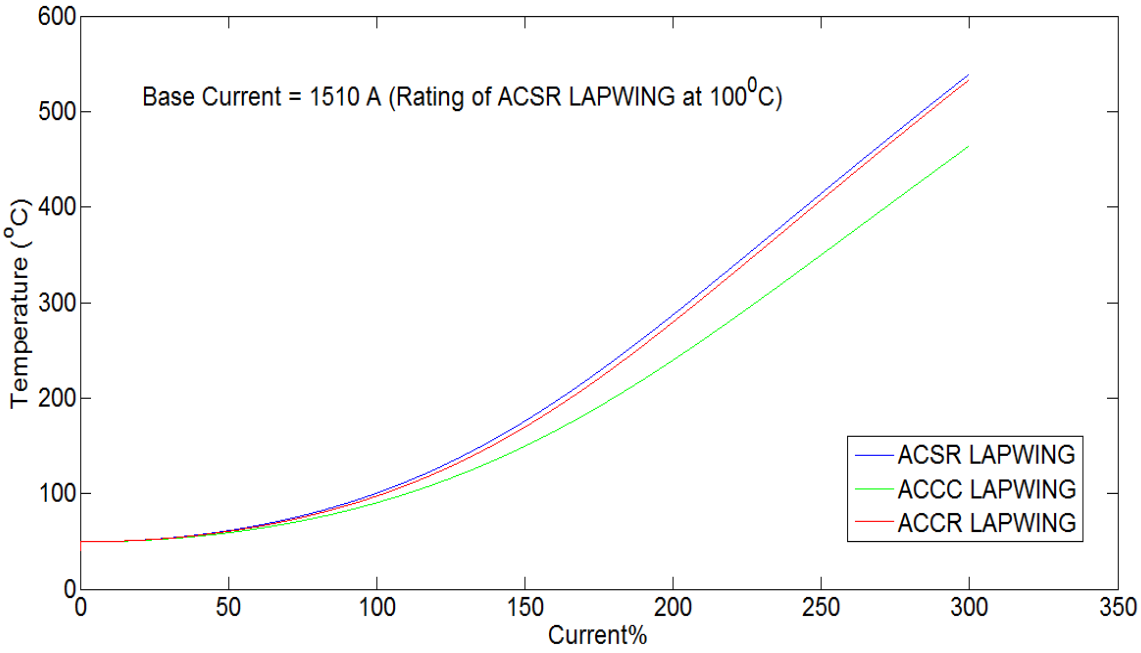

Fig 6.2 Current-temperature relationship of LAPWING sized conductors

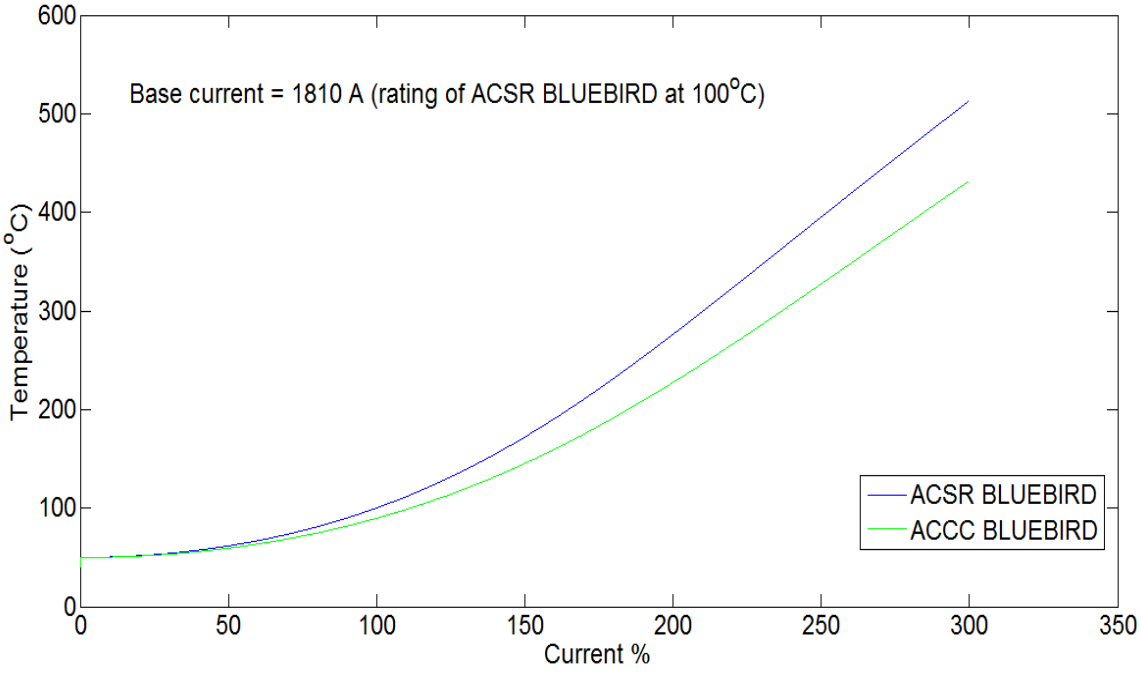

Fig 6.3 Current-temperature relationship of BLUEBIRD sized conductors

The current temperature relationship of the conductors reveals that in ACCC the temperature rise is low compared ACSR and ACCC at high temperatures in all the conductor sizes studied. ACCC has a superior current temperature relationship. The current temperature curves for ACSR and ACCR is similar but ACSR is thermally limited to 100°C whereas ACCR can operate continuously until 210°C. Thus, ACCR can carry more current than equivalent ACSR conductor can.

6.2 Transient thermal calculations

Transient thermal calculations were used to obtain the fault current – temperature curves of ACCC and ACCR conductors. The methodology for obtaining transient conductor temperature outlined in the IEEE 738 standard [21] was followed. A C++ program in Microsoft Visual Studio was developed to achieve the fault current – temperature calculations. The effect of fault currents of the order of 10 kA – 80 kA on the conductors was studied.

6.2.1 Non-steady-state heat balance

The non-steady-state heat balance equation is used to model the conductor temperature change in response to a step change of current flowing through the conductor [21]. For fault currents, this step increase is very large from initial operating current to final fault current. The ambient weather conditions are assumed to remain constant during the process of temperature change due to step change in the current. The conductor heat capacity influences the rate of temperature change. Equation (6.13) gives the non-steady state heat balance equation for a conductor carrying a transient current I (A) and having a resistance R (Ω/m) at temperature T_c (°C),

$$q_c + q_r + mC_p \frac{dT_c}{dt} = q_s + I^2 R(T_c) \quad (6.13)$$

Where,

q_c is the convection heat loss in W/m,

q_r is the radiation heat loss in W/m,

q_s is the solar heat gain in W/m,

$I^2 R(T_c)$ is the ohmic heat gain in W/m.

mC_p is the conductor heat capacity in W-s/(m-°C)

From equation (6.13), the rate of change of conductor temperature can be calculated as,

$$\frac{dT_c}{dt} = \frac{1}{mC_p}\left(q_s + I^2 R(T_c) - q_c - q_r\right) \quad (6.14)$$

The total heat capacity of the conductor is taken as the sum of the heat capacities of its constituent material. The product of its specific heat and the mass per unit length gives the heat capacity of the constituent materials of the conductor. However, for fault current calculations, the heat capacity of the core of the conductor is generally neglected for fault durations less than 60 seconds [21].

6.2.2 Fault current – temperature relationship of carbon composite core based conductors

Fault currents flowing through a conductor can quickly raise its temperature beyond permissible limits. Generally, fault currents are cleared in 3 – 5 cycles by the primary protection of the system. However, if the primary protection fails, then the backup protection operates in 0.2 – 0.5 seconds [60]. As described above, a C++ program was developed for obtaining the temperature rise of conductors subjected to fault currents

for any duration. This program was employed to give the temperature rise for DRAKE ACCC for fault currents of duration up to 5 seconds. The ambient weather conditions and the conductor material characteristics for DRAKE ACCC are given in Table 6.7

Table 6.7
Input parameters for fault current-temperature relationship of DRAKE ACCC conductor

Input parameters	Values
Wind Speed (m/s)	0.61
Elevation (m)	0
Emissivity	0.5
Solar Absoptivity	0.5
Ambient Temperature (°C)	40
Latitude (°)	43
Conductor diameter (mm)	28.1
Angle between conductor axis and wind direction (°)	90
Day number	161
Solar hour	14
AC resistance at 25°C (Ω/mile)	0.089
AC resistance at 75°C (Ω/mile)	0.106
Heat capacity of aluminum conductor (W-s/m-°C)	1289.34

The aluminum conductor of ACCC is produced from 1350 O – tempered aluminum [11]. The mass per unit length of the aluminum in DRAKE ACCC conductor is 1.4326 kg/km [61]. This gives a heat capacity of 1289.34 J/(m-°C) for the calculations.

The heat capacity of the core was neglected since the applied fault durations were less than 60 seconds in the simulation. Fault currents of 10 kA, 50 kA and 80 kA and duration up to 5 seconds were considered on DRAKE ACCC conductor operating initially at 125°C, 175°C and 200°C. The initial operating currents of the conductor are given in Table 6.8.

Table 6.8
Initial operating currents for DRAKE ACCC conductor

Temperature	Initial operating current
125°C	1354.08 A
175°C	1679.6 A
200°C	1813.33 A

Table 6.9 summarizes the results of the temperature rise on DRAKE ACCC conductor due to fault currents of 10 kA, 50 kA and 80 kA at different fault clearance times. Fig 6.4 gives the temperature rise for DRAKE ACCC conductor operating initially at 125°C, 175°C and 200°C under a fault current of 50 kA cleared in 0.55 seconds by backup protection. From the fault current – temperature relationship of DRAKE ACCC conductors, it can be concluded that,

1. If the fault current, of the order of 50 kA, is eventually cleared by the backup protection system, then the temperature in the conductor might rise above 250 °C.
2. The temperatures (≥250°C) exceed the glass transition temperature of the fully cured network of the epoxy matrix (T_{Ginf}), thus damaging to the fiber-matrix interface and permanently degrading the tensile strength of the conductor.

Table 6.9
Summary of temperature rise of DRAKE ACCC under different fault currents

Fault current (kA)	Initial operating temperature (°C)	Temperature at fault clearance times (°C)				
		3 cycles	5 cycles	0.583 s	1 s	5 s
10	125	125.3	125.5	128.5	131	155
	175	175.4	175.5	178.8	182	210
	200	200.4	200.6	204	206	235
50	125	132.5	137.5	222.5	310	2490
	175	185.5	189.3	286.5	384	2820
	200	209.1	215.1	318	420	2981
80	125	144	158	430.2	792	7897
	175	197.5	213	525	940	7898
	200	223.8	240.3	574	1004	7898

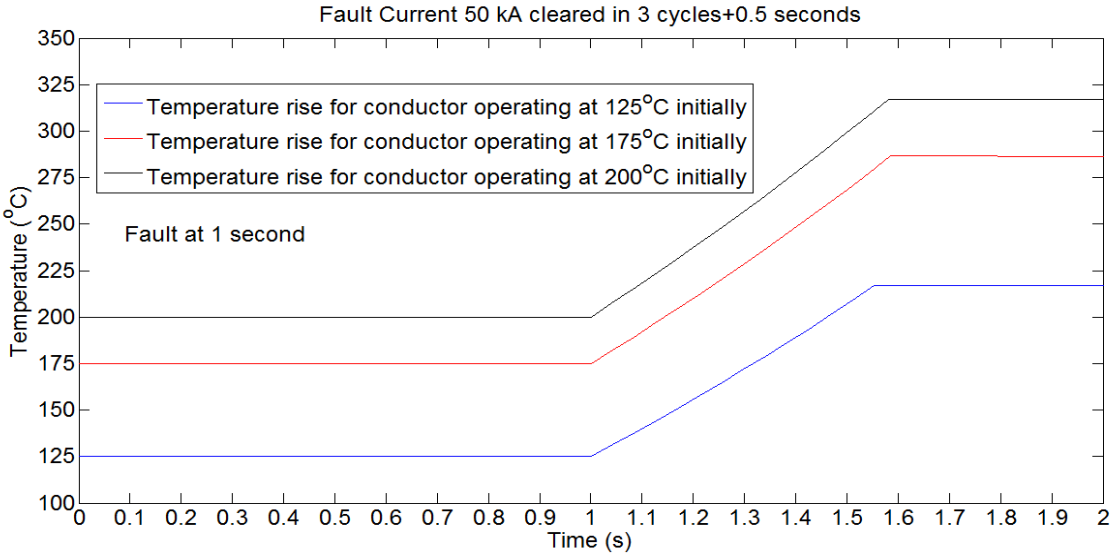

Fig 6.4 Fault current-temperature curves for DRAKE ACCC conductor

6.2.3 Fault current – temperature relationship of metal matrix core based conductors

Similar to the previous section, the temperature rise of metal matrix core based ACCR conductor due to fault currents was studied with the help of the developed C++ program. Ambient weather conditions and conductor characteristics, except the AC resistances and heat capacity of the aluminum conductor, given in Table 6.7 were considered. The value of AC resistance and heat capacity for DRAKE ACCR conductor considered in the calculations are given in Table 6.10. The initial operating currents of the conductor are given in Table 6.11.

Table 6.10
AC resistances and heat capacity of DRAKE ACCR conductor

AC resistance at 25°C (Ω/mile)	AC resistance at 25°C (Ω/mile)	Heat capacity of aluminum conductor (W-s/m-°C)
0.1126	0.1349	1062

Table 6.11
Initial operating currents for DRAKE ACCR conductor

Temperature	Initial operating current
125°C	1201.14 A
175°C	1488.47A
200°C	1606.36 A
240°C	1770 A

Table 6.12 summarizes the result of temperature rise on DRAKE ACCR conductor under fault currents of 10 kA, 50 kA and 80 kA of duration up to 10 seconds.

Table 6.12
Summary of temperature rise of DRAKE ACCR under different fault currents

Fault current (kA)	Initial operating temperature (°C)	Temperature at fault clearance times (°C)				
		3 cycles	5 cycles	0.583 s	1 s	10 s
10	125	125.4	125.7	131	135	227
	175	175.4	175.8	180.9	186	292
	200	200.5	200.9	206	210	257
	240	240.56	240.95	246	251	373
50	125	136.56	145	288	452	6225.7
	175	188.2	197	359	541	6225.7
	200	215	224	394	598.5	6225.7
	240	255	267	454	688.8	6225.7
80	125	155.4	177	700	1629.2	8626.8
	175	209	237	830	1888.6	8626.8
	200	237	261.5	893	1997.6	8626.8
	240	280	308	996	2209.3	8626.8

The conductor temperature reaches steady state within 10 seconds when exposed to a fault current of 50 kA or higher. Fig 6.5 gives the temperature rise for DRAKE

ACCR conductor operating initially at 125°C, 175°C, 200°C and 240°C under a fault current of 50 kA cleared in 0.55 seconds by backup protection.

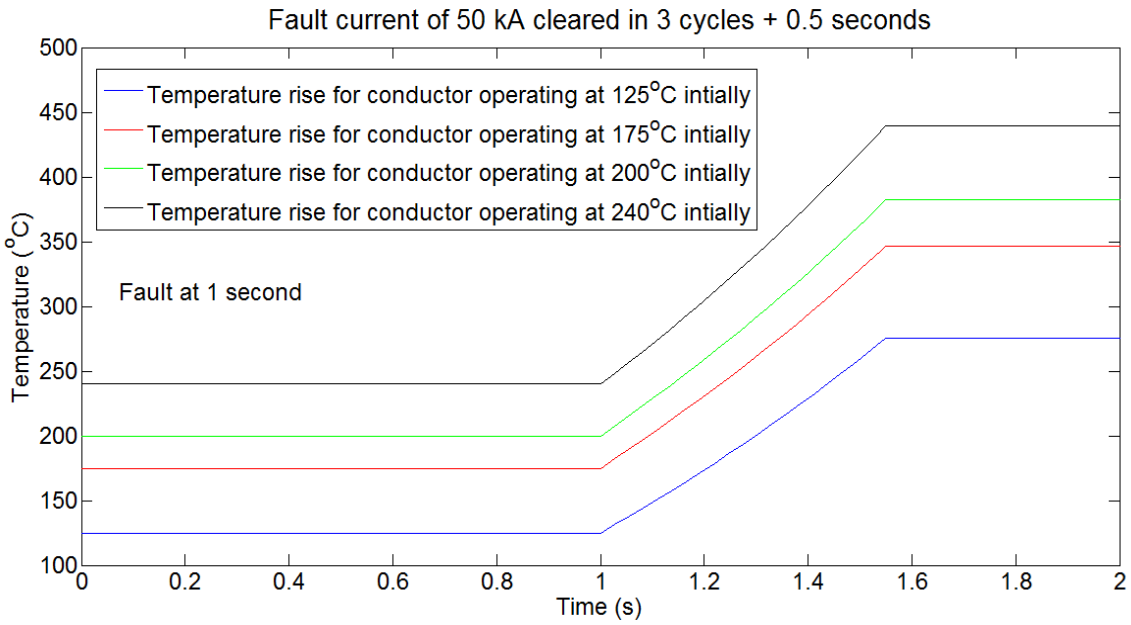

Fig 6.5 Fault current-temperature curves for DRAKE ACCR conductor

It can be seen from Table 6.12, the fault currents of the order of 80 kA can raise the temperature of DRAKE ACCR conductors above 650°C if the fault is cleared by backup protection in 0.583 seconds. The melting point of the aluminum matrix of ACCR is 650°C [59]. The alumina fibers of ACCCR conductor do not degrade in molten aluminum matrix since no chemical reaction occurs between alumina fibers and molten aluminum matrix [59]. However, it is important to investigate the residual strength of the conductor when the molten matrix solidifies after the clearance of the fault.

CHAPTER 7

CONCLUSION AND FUTURE WORK

7.1 Conclusions

The objective of this research is to characterize the mechanical properties of HTLS conductors with respect to temperature. HTLS conductors with carbon composite cores and metal matrix cores have been considered for the study. The work focused on the carbon composite core based conductors. Heat treatment of these conductor cores was performed to gauge the changes in its physical appearance and evolution of cracks with temperatures. Thermal mechanical analysis of the HTLS conductor cores provided information of its coefficient of thermal expansion. The loss of storage modulus (hence loss of tensile strength) of carbon composite cores with temperature was obtained with the help of the dynamic mechanical analysis. Dynamic mechanical analysis procedure provides a quick alternative to tensile testing of conductor at different temperatures to estimate the loss in tensile strength with temperature. The stress-strain behavior of metal matrix core was captured by conducting tensile testing. The current temperature relationships including fault currents for the HTLS conductors were developed using the IEEE 738-2006 standard. The programs were developed in C++ language in Microsoft Visual Studio suite. The calculations from these programs helped understand the set of conditions under which the conductors might accrue damage to its structure.

Chapter 2 described the heat treatment of carbon composite core based conductors. ACCC conductor core samples were exposed to isothermal environment at 125°C, 150°C, 200°C, 250°C and 300°C. The results of this experiment showed that the

ACCC conductor core can operate continuously at 125°C without the development of cracks either on carbon fiber/epoxy matrix and also on the glass-carbon fiber/epoxy interface. No cracking on the glass fiber/epoxy was observed. Isothermal environment at 150°C and above led to cracks on the carbon fiber/epoxy as well as fracture of the glass-carbon interface. The cracks and fractures increased in severity at temperatures 250°C and above. Radial cracks extending from the edge of the glass fiber/epoxy matrix section of the core to the glass-carbon interface were observed at this temperature. The ACCC conductor is designed to operate continuously at a maximum temperature of 180 °C with an emergency temperature of 200°C. However, cracks and fractures on the core are present from at least 150°C.

In chapter 3, the coefficients of thermal expansion of the metal matrix and carbon composite core of HTLS conductors were evaluated with the help of thermal mechanical analysis. The variations of the coefficient of thermal expansion of the cores with temperature were studied. The average coefficients of thermal expansion were also calculated in the temperature range of RT- 300°C. The average coefficient of thermal expansion of the metal matrix core was calculated to be $6\times10^{-6}/K$. The average coefficient of thermal expansion of carbon fiber/epoxy section of the carbon composite core was calculated to be $(-0.731)\times10^{-6}/K$. The thermal expansion coefficient of the metal matrix core is much higher than that of carbon composite core.

In chapter 4, dynamic mechanical analysis of the carbon fiber/epoxy samples sectioned from ACCC core were performed. Several samples were heat treated prior to the experiments. The results indicated that the storage modulus (hence tensile strength) of

the conductor core decreased about 65-70 % at 250 °C. Samples which were heat treated retained their storage modulus at room temperature after the heat treatment. The storage modulus characteristics improved with the degree of heat treatment of the samples, that is the rate of loss of storage modulus (hence tensile strength) with temperature decreased. This can be attributed to increased cross linked density of the epoxy matrix. However, the results showed that, the heat treatment at 250°C is just above the glass transition temperature of the fully cured network of the epoxy matrix. Thus, temperatures above 250°C will cause thermal degradation of the carbon composite core and reduce its mechanical strength by permanently damaging the fiber matrix interface.

In chapter 5, the tensile testing of metal matrix core was performed. The specimen, ACCC core strand was loaded successfully at 5 kN with the help of new custom grips. The custom gripping fixtures developed grips the sample with the help of friction force between the grips and the specimen. This friction occurs when the steel plate pushes on the split truncated cone, housing one end of the specimen, while it is inside the conical cavity of the steel box which compresses the upper end of the split truncated cone. This causes the split truncated cone to contact the specimen tightly and locks it down with the help of friction force. The stress strain curve of the metal matrix cone was also developed from the load displacement plot. The result indicated a presence of a yield point on the stress strain curve for the metal matrix core. The modulus of elasticity was calculated to be.

In chapter 6, the steady state thermal operation and transient thermal operation of metal matrix and carbon composite core based HTLS conductors were studied with the help of IEEE 738-2006 standard [21]. C++ programs were written in Microsoft Visual

Studio to perform the calculations. The steady state thermal calculation yielded the current temperature relationships of the HTLS conductor and the transient thermal calculation provided the fault current temperature relationship. The current temperature relationship indicates that ACCC conductor have superior current temperature characteristics than ACSR and ACCR conductors. The fault current temperature relationships reveal that for DRAKE ACCC, the temperature can rise above 250°C for fault current of the order of 50 kA cleared in 0.58 seconds by the backup protection. This can cause thermal degradation and permanent damage to the matrix and fiber matrix interface. On the other hand, the temperature rise for DRAKE ACCR is above 650°C for fault currents of the order of 80 kA cleared by the backup protection in 0.58 seconds. This will cause melting of the aluminum matrix of the conductor core. This may affect the residual tensile strength of the conductor after the core cools.

7.2 Future Work

The work done in this thesis focuses on the carbon composite core based HTLS conductors. Preliminary work has been done on the metal matrix core based conductor. Thus, much of the future research should be done in characterizing the metal matrix core based HTLS conductors. In this work loss of tensile strength of carbon composite core was estimated with the help of dynamic mechanical analysis indirectly through storage modulus. Tensile testing of the carbon composite core should be performed in order to validate the results from the dynamic mechanical analysis of the core. More research is required to perform tensile testing of metal matrix core at different temperatures to quantify the loss of tensile of the core with temperature.

REFERENCES

[1] U.S Energy Information Administration, "Annual energy outlook 2013 with projections to 2040," April 2013, available at: http://www.eia.gov/forecasts/aeo/pdf/0383(2013).pdf

[2] M. W. Chupka, R. Earle, P. Fox-Penner and R. Hledik, "Transforming America's power industry: The investment challenge 2010-2030," Nov. 2008, available at: http://www.eei.org/ourissues/finance/Documents/Transforming_Americas_Power_Industry_Exec_Summary.pdf

[3] Harris Williams & Co., "Transmission & distribution infrastructure," White Paper, Summer 2010, available at: http://www.harriswilliams.com/sites/default/files/industry_reports/final%20TD.pdf

[4] H. Huntington, "Electricity demand outlook: Now and in the future," Energy Modeling Forum Stanford University, Dec. 2009, available at: http://www.ncsl.org/documents/energy/HHuntington1209.pdf

[5] A. Alawar, E. J. Bosze and S. R. Nutt, "A composite core conductor for low sag at high temperatures," IEEE Transactions on Power Delivery, vol. 20, no. 3, pp. 2193 – 2199, July 2005.

[6] J. Lobry and D. Guery, "Theoretical study of dielectric breakdown in a new composite core HTLS conductor," IEEE Transactions on Power Delivery, vol. 7, issue 4, pp. 1862 – 1867, Oct. 2012.

[7] W. Torre, "Dynamic circuit thermal line rating," Oct. 1999, available at: http://www.energy.ca.gov/reports/2002-01-10_600-00-036.PDF

[8] K. S. Cory and B. G. Swezey, "Renewable portfolio standards in the States: Balancing goals and implementation strategies," Technical Report, NREL, Dec. 2007, available at: http://www.nrel.gov/docs/fy08osti/41409.pdf

[9] K. Dave, N. Mohan, D. Xianda, R. Gorur and R. Olsen, "Analyzing techniques for increasing power transfer in the electric grid," North American Power Symposium (NAPS), pp. 1 – 6, Sept. 2012.

[10] Electric Power Research Institute, " Demonstration of advanced conductors for transmission lines," Final Project Report, July 2008, available at: http://www.energy.ca.gov/2013publications/CEC-500-2013-030/CEC-500-2013-030.pdf

[11] ASTM conductor spec-sheets – CTC Global, available at: http://www.ctcglobal.com/images/uploads/main/ASTM_Conductor_Spec_Sheets.pdf

[12] 3M, "Aluminum conductor composite reinforced technical notebook (795 kcmil family): Conductor and accessory testing," available at: http://multimedia.3m.com/mws/mediawebserver?mwsId=66666UuZjcFSLXTtN8Tt4xfEEVuQEcuZgVs6E%20Vs6E666666

[13] J. Holman, "Increasing transmission capacity," Jan. 2011, available at: http://windsystemsmag.com/article/detail/191/increasing-transmission-capacity

[14] Notes on transmission facts, American Electric Power, available at: http://www.aep.com/about/transmission/docs/transmission-facts.pdf

[15] Notes on right-of-ways and easement for electric facility construction, Public Service Commission of Wisconsin, available at: http://psc.wi.gov/thelibrary/publications/electric/electric02.pdf

[16] Notes on project components and construction, operation and maintenance activities, available at: http://www.bpa.gov/Projects/Projects/I-5/draftEIS/DEIS%20Volume%201/Chapter%203%20Project%20Components.pdf

[17] R. S. Gorur, N. Chawla, J. Hunt and M. Dyer, "Mechanical and electrical issues concerning the use of composite materials for supporting core in transmission line conductors," IEEE Conference on Electrical Insulation and Dielectric Phenomena, pp. 501 – 504, Oct. 2006.

[18] V. T. Morgan, "Effect of elevated temperature operation on the tensile strength of overhead conductor," IEEE Transactions on Power Delivery, vol. 11, issue 1, pp. 345 – 352, Jan. 1996.

[19] Notes on TransPower® ACSR/TW bare overhead conductor, General Cable, available at: http://www.stabiloy.com/NR/rdonlyres/5263D5D3-D512-4934-9F2F-5B0DE99F41BC/0/GC_pg114120_TransPwr_ACSR_TW.pdf

[20] D. A. Douglass and R. Thrash, "Sag and tension of conductor," in Electric Power Generation, Transmission and Distribution, L. L. Grigsby, Ed. Boca Raton: CRC Press, 2012, ch. 14, pp. 1-42.

[21] *IEEE standard for calculating the current – temperature of bare overhead conductors*, IEEE Standard 738-2006, Jan. 2007.

[22] F. R. Thrash, "Transmission conductors – a review of the design and selection criteria," available at:

http://www.southwire.com/support/TransmissionConductoraReviewOfTheDesignandSelectionCriteria.htm

[23] J. R. Harvey, "Effect of elevated temperature operation on the strength of aluminum conductors," IEEE Transactions on Power Apparatus and Systems, vol. PAS-91, issue 5, pp. 1769 – 1772, Sept. 1972.

[24] B. R. Bogner, W. V. Breitigam, M. Woodward and K. L. Forsdyke, "Thermoset resins for pultrusion," in Pultrusion for Engineers, T. F. Starr, Ed. Boca Raton: CRC Press, 2000, ch. 4, pp. 97 – 174.

[25] D. J. Johnson, T. L. Anderson and H. E. Deve, "A new generation of high performance conductors," Power Engineering Society Summer Meeting, vol. 1, pp. 175 – 179, Jul. 2001.

[26] J. Hunt et al., "Composite conductor field trial summary report: ACCR 795-SRP-Phoenix, AZ field trial," 3M company, 2006, available at: http://multimedia.3m.com/mws/mediawebserver?mwsId=SSSSSufSevTsZxtUnx29ox_vevUqevTSevTSevTSeSSSSSS--&fn=ACCR795SRPFieldHED6-20-06.pdf

[27] P. Springer, "477-kcmil 3M brand composite conductor evaluation of materials from ORNL field test," 3M company, 2004, available at: http://multimedia.3m.com/mws/mediawebserver?mwsId=66666UF6EVsSyXTtOxT6NXTcEVtQEVs6EVs6EVs6E666666--&fn=72%20-%20477%20ACCR%20Post%20ORNL.pdf

[28] P. Springer, "1272-kcmil 3M™ composite conductor (ACCR) evaluation of materials from ORNL field test," 3M company, 2006, available at: http://multimedia.3m.com/mws/mediawebserver?mwsId=SSSSSuH8gc7nZxtUo8tSm8_1evUqe17zHvTSevTSeSSSSSS--&fn=69%20-%201272%20Post-ORNL.pdf

[29] T. Hill, "Experience and benefits of using high temperature low sag (HTLS) overhead conductors," 24th AMEU Technical Convention, Oct. 2013.

[30] Notes on customer installations, 3M company, available at: http://solutions.3m.com/wps/portal/3M/en_US/EMD_ACCR/ACCR_Home/CustomerInstall/CustomerInstall/

[31] T. Ishikawa, K. Koyama and S. Kobayashi, "Thermal expansion coefficients of unidirectional composites," Journal of Composite Materials, vol. 12, no. 2, pp.153 – 168, July 1978.

[32] D. E. Bowles and S. S. Tompkins, "Prediction of coefficients of thermal expansion for unidirectional composites," Journal of Composite Materials, vol. 23, no. 4, pp. 370 – 388, April 1989.

[33] R. Kulkarni and O. Ochoa, "Transverse and longitudinal CTE measurements of carbon fibers and their impact on interfacial residual stresses in composites," Journal of Composite Materials, vol. 40, no. 8, pp. 733 – 754, April 2006.

[34] B. Burks, D. L. Armentrout and M. Kumosa, "Failure prediction analysis of an ACCC conductor subjected to thermal and mechanical stresses," IEEE Transactions on Dielectrics and Electrical Insulation, vol. 17, issue 2, pp. 588 – 596, April 2010.

[35] C. McCullough, "Coefficient of thermal expansion for 477-T16 ACCR", 3M company, 2010, available at: http://multimedia.3m.com/mws/mediawebserver?mwsId=SSSSSufSevTsZxtUOY_UNxtvevUqevTSevTSevTSeSSSSSS--&fn=477%20Coeff%20of%20Thermal%20Expan.pdf

[36] T. Kavanagh and O. Armstrong, "An evaluation of high temperature low sag conductors for uprating the 220 kV transmission network in Ireland," 45th International Universities Power Engineering Conference (UPEC), pp. 1 -5, Sept. 2010.

[37] Composite Technology Corporation, "Development of stress – strain polynomials and creep parameters for ACCC/TW conductors", Feb. 2007, available at: http://www.powline.com/files/cables/ctc_conductors.pdf

[38] E. J. Bosze, A. Alawar, O. Bertschger, Yun-I. Tsai and S. R. Nutt, "High temperature strength and storage modulus in unidirectional hybrid composites," Composite Science and Technology, vol. 66, issue 13, pp. 1963 – 1969, Oct. 2006.

[39] J. Foreman, "Dynamic mechanical analysis of polymers," American Laboratory, Jan 1997, available at: http://www.tainstruments.com/pdf/literature/TA236.PDF

[40] K. P. Menard, "Dynamic mechanical analysis: A practical introduction," Boca Raton: CRC Press, 2008.

[41] M. Nakada, Y. Miyano, M. Kinoshita, R. Koga, T. Okuya and R. Muki, "Time-temperature dependence of tensile strength of unidirectional CFRP," Journal of Composite Materials, vol. 36, no. 22, pp. 2567 – 2581, Nov. 2002.

[42] Notes on dynamic mechanical analysis: a beginner's guide, Perkin Elmer, available at: http://www.perkinelmer.com/CMSResources/Images/44-74546GDE_IntroductionToDMA.pdf

[43] Notes on measurement of the glass transition temperature using dynamic mechanical analysis, TA Instruments, available at: http://www.tainstruments.com/pdf/literature/TS64.pdf

[44] A. Rossoll, B. Moser and A, Mortensen, "Tensile strength of axially loaded unidirectional Nextel 610™ reinforced aluminum: a case study in local load sharing between randomly distributed fibers," Composites Part A: Applied Science and Manufacturing, vol. 43, issue 1, pp. 129 – 137, Jan 2012.

[45] N. K. Kar, Y. I. Tsai, E. Barjasteh, E. J. Bosze and S. R. Nutt, "Accelerated aging and durability of composite rods for power transmission lines," available at: http://www.iccm-central.org/Proceedings/ICCM17proceedings/Themes/Industry/OTHER%20APPLICATIONS/A6.4%20Nutt.pdf

[46] E. Barjasteh, E. J. Bosze, Y. I. Tsai and S. R. Nutt, "Thermal aging of fiberglass/carbon-fiber hybrid composites," Composites Part A: Applied Science and Manufacturing, vol. 40, issue 12, pp. 2038 – 2045, Dec. 2009.

[47] R. Gorur, B. Mobasher and R. Olsen, "Characterization of composite cores for high temperature low sag (HTLS) conductors," PSERC Publication 09-05, July 2009.

[48] C. McCullough, "Thermal aging behavior and lifetime modeling for aluminum-zirconium alloy used in ACCR", 3M company, 2006, available at: http://multimedia.3m.com/mws/mediawebserver?mwsId=66666UgxGCuNyXTtOxT6Mxf_EVtQEcuZgVs6EVs6E666666--&fn=86%20-Aging%20StudyforAl-ZrWis.pdf

[49] C. McCullough, "Accelerated thermal aging behavior for aluminum-matrix composite wire used in the core for ACCR", 3M company, 2006, available at: http://multimedia.3m.com/mws/mediawebserver?mwsId=66666UF6EVsSyXTtOxT6MxMtEVtQEVs6EVs6EVs6E666666--&fn=99%20-%20Accelerated%20Aging%20Study.pdf

[50] L. Staszewski and W. Rebizant, "The differences between IEEE and CIGRE heat balance concepts for line ampacity considerations," Proceedings of the International Symposium Modern Electric Power Systems (MEPS), pp. 1 – 4, Sept. 2010.

[51] High temperature muffle furnace operation manual and parts list, Barnstead Thermolyne Corp., available at: http://www.nist.gov/ncnr/upload/E133thermolyne.pdf

[52] Anonymous, "Thermal analysis dilatometer- and TMA- evaluation with MS-Windows," Linseis Inc., Princeton Jct., NJ, Jan. 1998.

[53] Notes on Linseis – TMA/DMA L77, Linseis Inc., available at: http://www.linseis.net/html_en/thermal/tma/pdf/TMA_ENGISH.pdf

[54] Q 800 dynamic mechanical analysis brochure, TA Instruments, available at: http://www.tainstruments.com/pdf/brochure/dma.pdf

[55] A. B. Strong, "Understanding epoxies," Brigham Young University, available at: http://strong.groups.et.byu.net/pages/articles/articles/epoxies.pdf

[56] R. J. C. Carbas, L. F. M. da Silva, E. A. S. Marques and A. M. Lopes, "Effect of post cure on the glass transition temperature and mechanical properties of epoxy adhesives," Journal of Adhesion Science and Technology, vol. 27, issue 23, pp. 2542 – 2557, Apr. 2013.

[57] Instron model 4400 universal testing system user manual, available at: http://fab.cba.mit.edu/content/tools/instron/M10-94400-1.pdf

[58] Notes on stress-strain relationships, OPTI 222 Mechanical Design in Optical Engineering, available at: http://fp.optics.arizona.edu/optomech/references/OPTI_222/OPTI_222_W4.pdf

[59] N. Chawla and K. K. Chawla, "Metal matrix composites," New York: Springer, 2006.

[60] J. D. Glover, M. S. Sarma and T. J. Overbye, "Power system analysis & design," 5th ed. Delhi, India: Cengage Learning, 2012.

[61] J. R. Davies, "Aluminum and aluminum alloys," J. R. Davies & Associates, ASM International, 1993.

APPENDIX A

THERMAL MECHANICAL ANALYSIS RESULTS

A.1 Calculations for coefficient of thermal expansion of ACCR metal matrix core

The average coefficients of thermal expansion (CTE) for ACCR metal matrix core were calculated for each of the six tests. The change in length of the sample from room temperature to 300°C is also given. The calculations are given below,

Average CTE calculation for test 1:

$\Delta L = 16.52\ \mu m$ $T_{ini} = 19.5°C$ $T_{final} = 300°C$

$$\alpha_1 = \frac{\Delta L}{L\Delta T} = \frac{16.52\times10^{-6}}{10.1\times10^{-3}\times280.5} = 5.837\times10^{-6}/K \qquad (A.1.1)$$

Average CTE calculation for test 2:

$\Delta L = 16.72\ \mu m$ $T_{ini} = 20.8°C$ $T_{final} = 300°C$

$$\alpha_2 = \frac{\Delta L}{L\Delta T} = \frac{16.72\times10^{-6}}{10.1\times10^{-3}\times279.2} = 5.923\times10^{-6}/K \qquad (A.1.2)$$

Average CTE calculation for test 3:

$\Delta L = 17.78\ \mu m$ $T_{ini} = 20.2°C$ $T_{final} = 300°C$

$$\alpha_3 = \frac{\Delta L}{L\Delta T} = \frac{17.78\times10^{-6}}{10.1\times10^{-3}\times279.8} = 6.293\times10^{-6}/K \qquad (A.1.3)$$

Average CTE calculation for test 4:

$\Delta L = 15.81\ \mu m$ $T_{ini} = 17°C$ $T_{final} = 300°C$

$$\alpha_4 = \frac{\Delta L}{L\Delta T} = \frac{15.81\times10^{-6}}{10.1\times10^{-3}\times283} = 5.534\times10^{-6}/K \qquad (A.1.4)$$

Average CTE calculation for test 5:

$\Delta L = 16.4\ \mu m$ $T_{ini} = 18°C$ $T_{final} = 300°C$

$$\alpha_5 = \frac{\Delta L}{L\Delta T} = \frac{16.4\times10^{-6}}{10.1\times10^{-3}\times282} = 5.756\times10^{-6}/K \qquad (A.1.5)$$

Average CTE calculation for test 6:

$\Delta L = 17.58\ \mu m$ $T_{ini} = 21℃$ $T_{final} = 300℃$

$$\alpha_6 = \frac{\Delta L}{L\Delta T} = \frac{17.58\times10^{-6}}{10.1\times10^{-3}\times279} = 6.243\times10^{-6}/K \qquad \text{(A.1.6)}$$

A.2 Calculations for coefficient of thermal expansion of ACCC carbon composite core

The average coefficients of thermal expansion (CTE) for ACCC carbon composite core were calculated for each of the six tests. The change in length of the sample from room temperature to 300°C is also given. The calculations are given below,

Average CTE calculation for test 1:

ΔL = -2.23 μm T_{ini} = 17°C T_{final} = 300°C

$$\alpha_1 = \frac{\Delta L}{L\Delta T} = \frac{-2.23\times10^{-6}}{9.89\times10^{-3}\times283} = -0.799\times10^{-6}/K \qquad \text{(A.2.1)}$$

Average CTE calculation for test 2:

ΔL = -3.05 μm T_{ini} = 19.8°C T_{final} = 300°C

$$\alpha_2 = \frac{\Delta L}{L\Delta T} = \frac{-3.05\times10^{-6}}{9.89\times10^{-3}\times280.2} = -1.102\times10^{-6}/K \qquad \text{(A.2.2)}$$

Average CTE calculation for test 3:

ΔL = -0.54 μm T_{ini} = 17°C T_{final} = 300°C

$$\alpha_3 = \frac{\Delta L}{L\Delta T} = \frac{-0.54\times10^{-6}}{9.89\times10^{-3}\times283} = -0.193\times10^{-6}/K \qquad \text{(A.2.3)}$$

Average CTE calculation for test 4:

ΔL = -2.7 μm T_{ini} = 19.8°C T_{final} = 300°C

$$\alpha_4 = \frac{\Delta L}{L\Delta T} = \frac{-2.7\times10^{-6}}{9.89\times10^{-3}\times280.2} = -0.9744\times10^{-6}/K \qquad \text{(A.2.4)}$$

Average CTE calculation for test 5:

ΔL = -1.61 μm T_{ini} = 20.6°C T_{final} = 300°C

$$\alpha_5 = \frac{\Delta L}{L\Delta T} = \frac{-1.61\times10^{-6}}{9.89\times10^{-3}\times279.4} = -0.5836\times10^{-6}/K \qquad \text{(A.2.5)}$$

APPENDIX B

DYNAMIC MECHANICAL ANALYSIS RESULTS

B.1 Cambridge polymer DMA results

Several carbon fiber/epoxy matrix samples sectioned out from the ACCC carbon core were sent to Cambridge polymer Inc. for DMA testing. The temperature ramp rate for the DMA testing was 5°C/min and dual cantilever clamps were employed. The torque wrench used to secure the clamps with the sample was set to 9 in-lb. The amplitude and frequency of the oscillating force were 20 µm and 1 Hz respectively. The temperature range under investigation was room temperature - 300°C. The storage modulus, loss modulus and the tan delta curve of the sample as a function of the temperature is given in Fig B.1.1. Table B.1.1 presents some corresponding data points for the curves.

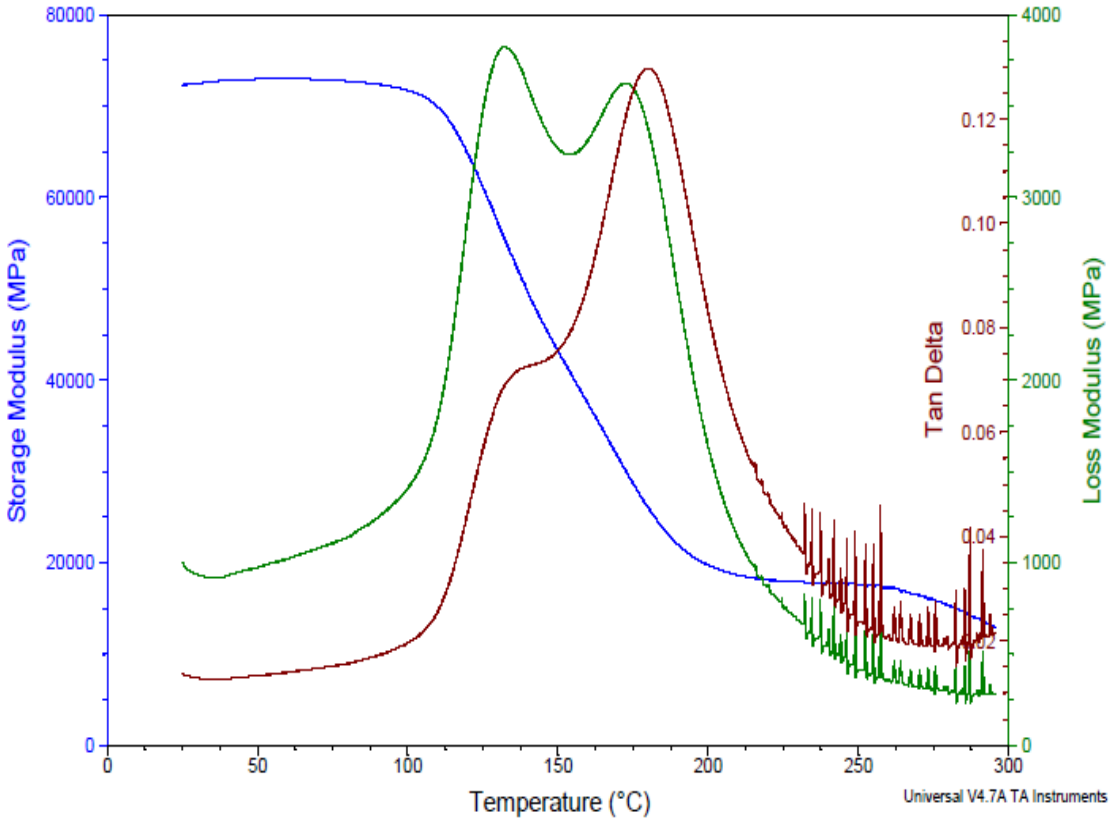

Fig B.1.1 Storage modulus, loss modulus and tan delta curves with temperature for untreated ACCC carbon fiber/epoxy sample.

Table B.1.1
Storage modulus, loss modulus and tan delta at various temperatures

Temperature (°C)	Storage modulus (MPa)	Loss modulus (MPa)	Tan delta
75.05	72833	1108	0.02
132.12	55568	3825	0.07
172.60	30048	3625	0.12
250.12	17591	416	0.02

B.2 Standard deviation, relative standard deviation for storage modulus curves and tan delta values

The maximum, minimum and average standard deviation of the storage modulus curves obtained in the DMA tests for virgin and heat treated samples were calculated. The relative standard deviation of the storage modulus curves from these tests from the mean storage modulus curve is also presented. Similarly, the standard deviation and relative standard deviation of the values of tan delta peak gathered from the experiments is given here. Table B.2.1 and table B.2.2 provides the standard deviation and relative standard deviation values.

Table B.2.1
Minimum, maximum, average and relative standard deviation of the storage modulus curves

Type of sample	Minimum S.D (MPa)	Maximum S.D (MPa)	Temperature at minimum S.D (°C)	Temperature at maximum S.D (°C)	Average S.D (MPa)	Relative S.D (%)
Virgin sample	674	4485	295	139	2164.2	8.15
125°C sample	962.34	6405.8	294	30	3908.6	13.18
175°C sample	1510.9	5344	295	157	3076.1	9.1
250°C sample	1187.4	3964.7	295	145	3076	7.33

Table B.2.2
Tan delta mean, standard deviation and relative standard deviation of the tan delta values

Type of sample	Tan delta mean	Standard deviation	Relative standard deviation (%)
Virgin sample	0.1275	0.0023	1.8
125°C sample	0.1151	0.0087	7.56
175°C sample	0.095	0.0059	6.21
250°C sample	0.1254	0.0064	5.1